

THESIS FOR THE DEGREE OF DOCTOR OF PHILOSOPHY

Estimation of Forest Biomass and Faraday Rotation using Ultra High
Frequency Synthetic Aperture Radar

GUSTAF SANDBERG

Department of Earth and Space Sciences

CHALMERS UNIVERSITY OF TECHNOLOGY
Gothenburg, Sweden 2013

Estimation of Forest Biomass and Faraday Rotation using Ultra High Frequency
Synthetic Aperture Radar
GUSTAF SANDBERG
ISBN 978-91-7385-912-7

© GUSTAF SANDBERG, 2013.

Doktorsavhandlingar vid Chalmers tekniska högskola
Ny serie nr 3593
ISSN 0346-718X

Department of Earth and Space Sciences
Chalmers University of Technology
SE-412 96 Gothenburg
Sweden
Telephone + 46 (0)31-772 1000

Cover:

The cover illustration shows biomass change maps based on airborne high density laser scanning data and simulated data for a spaceborne P-band SAR data similar to BIOMASS at two different spatial resolutions. The image is reproduced from Figure 5 in paper V, but with the legend label changed from logarithmic to percentage scale.

Printed by Chalmers Reproservice
Gothenburg, Sweden 2013

Estimation of Forest Biomass and Faraday Rotation using Ultra High Frequency Synthetic Aperture Radar

GUSTAF SANDBERG

Department of Earth and Space Sciences
Chalmers University of Technology

ABSTRACT

Synthetic Aperture Radar (SAR) data in the Ultra High Frequency (UHF; 300 MHz – 3 GHz) band have been shown to be strongly dependent of forest biomass, which is a poorly estimated variable in the global carbon cycle. In this thesis UHF-band SAR data from the fairly flat hemiboreal test site Remningstorp in southern Sweden were analysed. The data were collected on several occasions with different moisture conditions during the spring of 2007. Regression models for biomass estimation on stand level (0.5-9 ha) were developed for each date on which SAR data were acquired. For L-band (centre frequency 1.3 GHz) the best estimation model was based on HV-polarized backscatter, giving a root mean squared error (rmse) between 31% and 46% of the mean biomass. For P-band (centre frequency 340 MHz), regression models including HH, HV or HH and HV backscatter gave an rmse between 18% and 27%. Little or no saturation effects were observed up to 290 t/ha for P-band. A model based on physical-optics has been developed and was used to predict HH-polarized SAR data with frequencies from 20 MHz to 500 MHz from a set of vertical trunks standing on an undulating ground surface. The model shows that ground topography is a critical issue in SAR imaging for these frequencies. A regression model for biomass estimation which includes a correction for ground slope was developed using multi-polarized P-band SAR data from Remningstorp as well as from the boreal test site Krycklan in northern Sweden. The latter test site has pronounced topographic variability. It was shown that the model was able to partly compensate for moisture variability, and that the model gave an rmse of 22-33% when trained using data from Krycklan and evaluated using data from Remningstorp. Regression modelling based on P-band backscatter was also used to estimate biomass change using data acquired in Remningstorp during the spring 2007 and during the fall 2010. The results show that biomass change can be measured with an rmse of about 15% or 20 tons/ha. This suggests that not only deforestation, but also forest growth and degradation (e.g. thinning) can be measured using P-band SAR data.

The thesis also includes result on Faraday rotation, which is an ionospheric effect which can have a significant impact on spaceborne UHF-band SAR images. Faraday rotation angles are estimated in spaceborne L-band SAR data. Estimates based on distributed targets and calibration targets with high signal to clutter ratios are found to be in very good agreement. Moreover, a strong correlation with independent measurements of Total Electron Content is found, further validating the estimates.

APPENDED PAPERS

This thesis is based on the work contained in the following papers, referred to by Roman numerals in the text:

- I Sandberg, G., Eriksson, L. E. B., and Ulander, L. M. H. (2009), “Measurements of Faraday rotation using polarimetric PALSAR images”, *IEEE Geoscience and Remote Sensing Letters* **6**(1), 142-146.
- II Hallberg, B., Smith-Jonforsen, G., Ulander, L. M. H., and Sandberg, G. (2008), “A physical-optics model for double-bounce scattering from stems standing on an undulating ground surface”, *IEEE Transactions on Geoscience and Remote Sensing* **46**(9), 2607-2621.
- III Sandberg, G., Ulander, L. M. H., Holmgren, J., Fransson, J. E. S., and Le Toan, T. (2011), “L- and P-band backscatter intensity for biomass retrieval in hemiboreal forest”, *Remote Sensing of the Environment* **115**(11), 2874-2886.
- IV Soja, M. J., Sandberg, G., and Ulander, L. M. H. (2013), “Regression-based retrieval of boreal forest biomass in sloping terrain using P-Band SAR backscatter intensity data”, *IEEE Transactions on Geoscience and Remote Sensing* **51**(4), 2646-2665.
- V Sandberg, G., Ulander, L. M. H., Wallerman, J., and Fransson, J. E. S., “Measurements of forest biomass change using P-band SAR backscatter”, *submitted to IEEE Transactions on Geoscience and Remote Sensing*

ADDITIONAL PUBLICATIONS

Besides the appended papers, the author has contributed to the following publications. They have not been appended in the thesis because my most important work is contained the appended papers, but they are listed here for completeness.

- A. Kononov, A., Wyholt, A., Sandberg, G., and Ulander, L. M. H. (2011), “Statistical Analysis of VHF-Band Tree Backscattering Using Forest Ground Truth Data and PO Scattering Model”, *IEEE Transactions on Geoscience and Remote Sensing* **49**(8), 3035-3046.
- B. Hajnsek, I., Scheiber, R., Ulander, L. M. H., Gustavsson, A., Sandberg, G., Tebaldini, S., Guarnieri, A. M., Rocca, F., Bombardini, F., and Pardini, M. (2008), “BioSAR 2007 technical assistance for the development of airborne SAR and geophysical measurements during the BioSAR 2007 experiment: final report without synthesis”, Technical report, European Space Agency, Contract no.: 20755/07/NL/CB.
- C. Hajnsek, I., Scheiber, R., Keller, M., Horn, R., Lee, S., Ulander, L. M. H., Gustavsson, A., Sandberg, G., Le Toan, T., Tebaldini, S., Guarnieri, A. M., and Rocca, F. (2009), “BioSAR 2008 technical assistance for the development of airborne SAR and geophysical measurements during the BioSAR 2008 experiment: draft final report – BioSAR campaign”, Technical report, European Space Agency, Contract no.: 22052/08/NL/CT.
- D. Ulander, L. M. H., Gustavsson, A., Flood, B., Murdin, D., Dubois-Fernandez, P., Depuis, X., Sandberg, G., Soja, M. J., Eriksson, L. E. B., Fransson, J. E. S., Holmgren, J., and Wallerman, J. (2011), “BioSAR 2010 technical assistance for the development of airborne SAR and geophysical measurements during the BioSAR 2010 experiment: Final report”, Technical report, European Space Agency, Contract no.: 4000102285/10/NL/JA/ef.
- E. Le Toan, T., Angelliaume, S., Borderies, P., Couhert, A., Dubois-Fernandez, P., Garestier, F., Hoekman, D., Kugler, F., Lee, S. K., Papathanassiou, K., Petrucci, B., Quinones, M., Sandberg, G., Ulander, L. M. H., Valteau, J., and Villard, L. (2011), “P-band SAR wave interaction and information retrieval Analysis and inversion of P-band SAR data for forest biomass and height mapping”, Technical report, European Space Agency, Contract no.: 20290/06/NL/LvH.
- F. Papathanassiou, K., Balzter, H., Eriksson, L. E. B., Gustavsson, A., Kugler, F., Lee, S. K., Sauer, S., Sandberg, G., Soja, M. J., Scheiber, R., Le Toan, T., Ulander, L. M. H., and Villard, L. (2012), “Development of algorithms for biomass retrieval”, Technical report, European Space Agency, contract no.: 4200023081/NL/AF.
- G. ESA (2012), “Report for Mission Selection: Biomass”, ESA SP-1324/1 (3 volume series). Noordwijk, Netherlands: European Space Agency.

ACKNOWLEDGEMENTS

First and foremost I would like to extend my very deep gratitude towards my main supervisor Lars Ulander. Through many discussions and through continued support, he has enabled me to fill this thesis with what I hope is a useful contribution to the field. My thanks and gratitude also goes to my co-supervisors Leif Erikson and Johan Fransson, who have lent me their invaluable support.

I would also like to thank my past and present colleagues in the radar remote sensing group. Special thanks go to Maciej Soja, Klas Alenljung, Gary Smith-Jonforsen, Björn Hallberg and Jan Askne, with whom I have collaborated in the field of SAR for forestry applications. Assistance provided by several fellow researchers at the Swedish University of Agricultural Sciences, in particular by Johan Holmgren and Jörgen Wallerman, was greatly appreciated. Thanks also to my colleagues at the Department of Earth and Space Sciences, for making this a wonderful place to work.

Thanks to the Swedish National Space Board (SNSB) and to the European Space Agency (ESA) for providing the funding for this thesis.

Warm thanks also go to my family and friends, who have encouraged and supported me both before and during my PhD-studies. Each of you holds a special place in my heart. Finally my unending gratitude and love goes to my beautiful wife and my lovely children. To you I dedicate this thesis, and my life.

TABLE OF CONTENTS

ABSTRACT.....	III
APPENDED PAPERS.....	V
ADDITIONAL PUBLICATIONS.....	VI
ACKNOWLEDGEMENTS	VII
Table of Contents.....	IX
1 Introduction	1
1.1 Radar Remote Sensing	1
1.1.1 Frequency Band Letter Designations.....	1
1.1.2 Polarizations	2
1.2 Synthetic Aperture Radar	3
1.3 Forest Biomass	3
1.3.1 The Global Carbon Cycle	3
1.3.2 Measuring Biomass on a Global Scale	4
1.4 UHF SAR for Biomass Mapping	7
1.4.1 The BIOMASS Mission	7
1.5 Scope of this Thesis.....	8
2 Radar Imaging	9
2.1 Radar Principles	9
2.1.1 Basic Sub-systems	9
2.1.2 Radiometry	9
2.1.3 Range Resolution	10
2.1.4 Phase Measurements	10
2.1.5 Range-Doppler Ambiguity.....	10
2.2 SAR Image Formation	11
2.2.1 Ambiguity Considerations in Spaceborne SAR	12
2.2.2 Interferometry and Tomography.....	12
2.3 Speckle.....	13
2.4 Radiometric SAR Calibration.....	15
2.5 Examples of SAR Systems.....	15
2.5.1 CARABAS-II and LORA	15

2.5.2	E-SAR.....	16
2.5.3	SETHI.....	16
2.5.4	ALOS PALSAR.....	16
2.5.5	BIOMASS.....	16
3	Ionospheric Disturbances.....	17
3.1	The Ionosphere.....	17
3.2	Impact on SAR Observables.....	17
3.2.1	Background Ionosphere.....	17
3.2.2	Scintillations.....	19
3.3	Overview of Correction Methods.....	20
3.3.1	Faraday Rotation.....	20
3.3.2	Scintillation.....	21
3.4	Summary of Paper I.....	22
3.5	Conclusions and Outlook.....	23
4	UHF SAR for Biomass Mapping.....	25
4.1	What Affects the Scattering?.....	25
4.2	Physical Forest Scattering Models.....	27
4.2.1	Summary of Paper II.....	28
4.3	Empirical Estimation Models.....	28
4.3.1	Empirical and Semi-empirical Models.....	29
4.3.2	Model Selection and Evaluation.....	30
4.3.3	Overview of Regression Based Studies.....	34
4.3.4	Summary of Paper III.....	37
4.3.5	Summary of Paper IV.....	38
4.3.6	Discussion and Conclusions.....	39
4.4	Biomass Change.....	39
4.4.1	Summary of Paper V.....	39
4.4.2	Conclusions and Outlook.....	40
4.5	Summary and Conclusions.....	40
5	Conclusions and Outlook.....	42
6	References.....	44

1 INTRODUCTION

This thesis is motivated by the need for improved estimates of forest biomass. Evidence suggests that radar imaging, in particular Synthetic Aperture Radar (SAR) imaging in the Ultra High Frequency (UHF)-band, is a very useful tool to obtain reliable estimates of forest biomass and forest biomass change on a global scale. In this thesis data from several airborne campaigns have been used to improve and evaluate such estimates. Faraday rotation is an important issue when UHF-band SAR systems are placed on spaceborne platforms. The ionosphere affects the propagating electromagnetic waves, and distorts the SAR images. Faraday rotation is one such distortion effect. In this thesis Faraday rotation is estimated in SAR data from a spaceborne UHF-band SAR.

The outline of the thesis is as follows. In the remainder of this section the concepts radar, SAR and biomass are described, and the scope and motivation for the thesis are given. In section 2 some technical concepts underlying radar imaging are described. Section 3 deals with ionospheric disturbances, as well as correction methods for such disturbances. In section 4 the major part of the thesis is presented, namely biomass mapping using UHF-band SAR. Finally, conclusions and an outlook are presented in section 5.

1.1 RADAR REMOTE SENSING

Radar is an acronym for radio detection and ranging. Radars are active systems, in the sense that they do not rely on other sources of electromagnetic radiation. Thus, radars can operate both day and night. Radars operate in a wide range of frequencies from a few MHz to hundreds of GHz. For a large part of this spectrum the electromagnetic waves can propagate through clouds, haze and rain. When imaging the Earth's surface this is a strong benefit, since radars images are unaffected by cloud cover. Radars have many applications, both civilian and military. This thesis concerns radar for remote sensing purposes. Remote sensing is a broad term, defining activities where physical objects are "sensed" by some measurement system which is "remotely separated" from the physical object. Typical remote sensing applications include atmospheric measurements and imaging of the Earth's surface by means of satellite instruments.

1.1.1 FREQUENCY BAND LETTER DESIGNATIONS

The radio spectrum is divided into several letter designated frequency bands by the International Telecommunications Union (ITU) (ITU, 2012). Specialized letter designations for radar applications are also commonly used (IEEE, 2003). Table 1 gives a comparison of the nomenclature used by the radar community and the nomenclature used in the broader telecommunications field. Note that P-band, which is commonly used in radar remote sensing, is not defined. However, it is noted in IEEE (2003) that frequencies from 216-450 MHz are sometimes called P-band. Note also that the definition of UHF differs in the two nomenclatures. In this thesis we adopt the

more general ITU definition and include frequencies between 300 MHz to 3 GHz (0.1 m to 1 m wavelength) in the UHF-band. Thus, both the P- and L-bands are included in the UHF-band, except for the lower part of the P-band. In particular, all SAR data used in this thesis are contained in the UHF-band, except VHF band data included in paper II.

Table 1. Comparison of radar-frequency letter band nomenclature with ITU nomenclature. Adopted from IEEE (2003).

Radar nomenclature		ITU nomenclature			
Radar letter designation	Frequency range	Frequency range	Band No.	Adjectival band designation	Corresponding metric designation
HF	3-30 MHz	3-30 MHz	7	High frequency (HF)	Dekametric waves
VHF	30-300 MHz	30-300 MHz	8	Very High Frequency (VHF)	Metric waves
UHF	300-1000 MHz	0.3-3 GHz	9	Ultra High Frequency (UHF)	Decimetric waves
L	1-2 GHz				
S	2-4 GHz				
C	4-8 GHz	3-30 GHz	10	Super High Frequency (SHF)	Centimetric waves
X	8-12 GHz				
Ku	12-18 GHz				
K	18-27 GHz				
Ka	27-40 GHz	30-300 GHz	11	Extremely High Frequency (EHF)	Millimetric waves
V	40-75 GHz				
W	75-110 GHz				
mm	110-300 GHz				

1.1.2 POLARIZATIONS

One of the basic properties of electromagnetic (EM) waves is the polarization (see e.g. Goldstein (2003)). The polarization describes the orientation of oscillation of the wave's electric field. An EM wave propagating in free space can always be partitioned into two orthogonal polarization states (polarization basis). Common polarization basis are horizontal (H) and vertical (V) polarization (linear polarization), of left- and right hand circular polarizations. Radar systems both transmit and receive EM waves. Thus, a polarization state is defined both on transmission and reception. Fully polarimetric systems are able to both transmit and receive both states in a polarization basis. For a linear polarization basis it is common to use the terms HH (horizontal transmit and receive), VV (vertical transmit and receive) and cross-polarization (HV or VH, horizontal or vertical transmit and reception of the other component).

1.2 SYNTHETIC APERTURE RADAR

An important parameter in imaging radars is the spatial resolution. Resolution in two (or three) dimensions is required when imaging the Earth's surface. For a side-looking radar, i.e. a radar that transmits energy in a direction perpendicular to the line of flight, the along-track resolution is determined by the transmitted wavelength divided by the length of the antenna and multiplied by the distance to the imaged scene. In the UHF-band (0.1 m to 1 m wavelength) very large antennas are required to obtain good resolution. For spaceborne systems constraints on antenna size and long distance to targets restricts the resolution of UHF systems to kilometre scales. Synthetic Aperture Radar is a technique to overcome this limitation (Brown, 1967). If the radar transmits a train of pulses for which the relative phases are known, signal processing can be used to synthesize an antenna much larger than the physical antenna. Using this technique the resolution in the along-track direction can be brought down to meter scale or below even for spaceborne systems.

1.3 FOREST BIOMASS

The most significant motivation for wanting to measure biomass on a global scale is due to its role in the global carbon cycle (ESA, 2012). As is commonly known mankind has significantly altered the level of carbon dioxide in the atmosphere, which in turn leads to climate warming. Dealing with this threat to our climate is perhaps one of the most important tasks of the global community. While the decisions needed to mitigate climate warming lie in areas of politics and economics (far beyond the scope of this thesis), it is essential that the scientific community provides understanding of the processes underlying this threat to our climate. In this context the ability to model the global carbon cycle with low error is an important piece of the puzzle.

1.3.1 THE GLOBAL CARBON CYCLE

The carbon cycle can be characterized by the rate of change in atmospheric carbon dioxide (flux), partitioned in different parts of the climate system. Mankind contribute directly to these fluxes (i.e. a source) by emissions from fossil fuels, but also indirectly by land use change (e.g. deforestation). The terrestrial ecosystem also absorbs carbon (i.e. a sink) in a process which is poorly understood (IPCC, 2007). The final important component of the carbon cycle is the oceans, which act as a sink. The fluxes for the different components are constrained by the overall net flux to the atmosphere, which can be measured independently with low error.

Estimated fluxes to the atmosphere and associated errors are presented in Table 2. Largest uncertainties are found in the ocean and land fluxes, both of which act as a sink. However, there is a large difference in how estimates for the size of the land and ocean sinks are derived. The ocean sink is derived from models and observations, which also give an error estimate. The net land to atmosphere flux is instead derived by subtracting the ocean sink from the total sink. Its errors are also determined indirectly by error propagation (IPCC, 2007). The land sink can be partitioned into a source term

due to land use change and a residual terrestrial sink. Only the source term can be estimated. The sink is inferred from the net land to atmosphere flux and the land use flux.

Table 2. The global carbon budget in $GtCyr^{-1}$, reproduced from (ESA, 2012). The error represent ± 1 standard deviation estimates. The uncertainties in the source and sink terms making up the net land to atmosphere flux are large and indicated only as ranges.

	1980-1989	1990-1999	2000-2009
Atmospheric increase	3.3 ± 0.1	3.2 ± 0.1	4.1 ± 0.1
Emissions (fossil fuel and cement)	5.4 ± 0.3	6.4 ± 0.4	7.9 ± 0.4
Net ocean to atmosphere flux	-1.8 ± 0.8	-2.2 ± 0.4	-2.3 ± 0.5
Net land to atmosphere flux	-0.3 ± 0.9	-1.0 ± 0.6	-1.5 ± 0.6
The net land to atmosphere flux is partitioned as			
Land-use change flux	1.4 (0.4 to 2.3)	1.6 (0.5 to 2.7)	1.1 (0.3 to 2.8)
Residual terrestrial sink	-1.7 (-3.4 to 0.2)	-2.6 (-4.3 to -0.9)	-2.5 (-4.2 to -0.9)

The observations above clearly illustrate that the lack of knowledge of the terrestrial part of the carbon flux is great. Forest biomass comprise about 70-90% of the Earth's above ground biomass (ESA, 2012). One of the great sources of uncertainty lies in the currently poor measurements of forest biomass stock, forest degradation and deforestation, and forest growth. Therefore there is a strong need for improved methods for biomass mapping and monitoring.

1.3.2 MEASURING BIOMASS ON A GLOBAL SCALE

Mapping forest biomass and forest biomass change is not only important as a means to reduce errors in the global carbon cycle. Forests also have great economic, biological, environmental and recreational values. Such values are easier to preserve and manage with access to reliable forest biomass maps.

Forest biomass is defined as the dry weight of woody matter and leaves/needles, and is usually measured in units of Mg/ha or tons/ha (also denoted t/ha). The total forest biomass is the sum of the biomass located above ground (e.g. trunk and branches) and below ground (root system). Within the scope of this thesis forest biomass is defined as above ground biomass (AGB).

Forest biomass can only be measured directly by harvesting, drying and weighing the harvested material. This method is necessary for establishment of so called allometric equations, i.e. equations relating *in-situ* measurements to biomass. However, it is obvious that destructive harvesting cannot be used to measure forest biomass on a global scale. Instead indirect methods must be employed to estimate forest biomass.

Such estimation methods can be classified into two broad categories: *in-situ* measurements and remote sensing techniques.

The first of these techniques relies on *in-situ* measurements of e.g. tree height and diameter, tree age, tree species and classification of growth conditions. Measurements are usually made within measurement plots (or elongated transects). Allometric equations are then used to estimate forest biomass for the plots, and the plot level data are then used to estimate forest biomass on larger scales. Errors in biomass estimates based on *in-situ* data arise from two main sources. First, allometric equations give errors on tree level. These errors may be both systematic (bias) or random. These errors tend to be larger for heterogeneous multi-species forests (e.g. tropics) than in homogeneous managed forest with only few species. The second type of error arises when plot level data are up-scaled to larger areas. Unbiased up-scaling relies on the assumption that the plot level data are representative samples of the larger biomass “population”, and that the number of plots are sufficiently large to produce reliable estimates. Both of these conditions are easier to fulfil in homogeneous forests. Strong heterogeneity implies that the plots must be both large and numerous. Large plots are especially important in the tropics, where plot sizes in the order of 1 ha are required (Saatchi et al., 2011). An additional source of error in plot level measurements of *in-situ* biomass is associated with the determination of the plot area. In some circumstances, e.g. topographic terrain with dense understory, it may be difficult to exactly determine the boundaries of the plot in the field. Post processing based on position measurements in field is also associated with errors. Since biomass is a density measure, errors in plot area directly affects biomass estimates. In cases when other error sources are small (e.g. good allometric equations are available), such errors should be given proper attention.

In Europe, Canada and USA there exists large national inventories of *in-situ* measurements, while in other parts of the world there are only limited *in-situ* data available. *In-situ* measurements can only provide forest biomass data with coarse spatial and temporal resolution. Compared to *in-situ* measurements, remote sensing techniques can provide better temporal and spatial resolution as well as coverage. There are several different remote sensing techniques for estimation of forest biomass. On local to regional scales airborne high density laser scanning can be used to provide estimates of forest biomass with low estimation errors (Koch, 2010). However, high density laser scanning data are costly and time-consuming to collect and cannot be used on a global scale. Satellite based laser systems can also be used for biomass estimation (Lefsky et al., 2005), but global coverage is limited to transects. Optical data from satellite imagery suffer from weak sensitivity to forest biomass at high biomass levels (saturation). SAR backscatter data using frequencies above the UHF-band has been shown to saturate at low levels of biomass (Imhoff, 1995b). However, recent attempts have been made to use long time series of C-band satellite data used to map boreal forests (Santoro et al., 2011; Santoro et al., 2013). At a resolution of 1 km the relative estimation error was found to be about 50% or less. Spaceborne

interferometric C-band measurements have been modelled based on forest variables, and the model has been inverted to obtain forest stem volume (Askne et al., 1997; Santoro et al., 2002; Askne et al., 2003). This method has given promising results in some test sites, but at present there are no spaceborne SAR systems capable of interferometric C-band imaging. Repeat-pass interferometric measurements from Siberian forest acquired by the L-band satellite J-ERS are analysed in Eriksson et al. (2003) and Eriksson (2004). The analysis showed a clear correlation between JERS coherence and forest growing stock volume during winter conditions, while during summer results were unreliable. During spring and fall temporal decorrelation caused large problems. High resolution interferometric X-band data are currently provided by TanDEM-X and COSMO-SkyMed (Krieger et al., 2007; Covello et al., 2012). Recent results have shown that such data can be used for forest biomass estimation (Caicoya et al., 2012). However, neither TanDEM-X nor COSMO-SkyMed provides global coverage, and the main sensitivity is to forest height rather than biomass.

Several studies have shown that HH-polarized VHF band SAR backscatter has a very strong sensitivity to forest stem volume (Israelsson et al., 1997; Israelsson, 1998; Fransson, 1999; Fransson et al., 2000; Melon et al., 2001). Dependence on stem volume implies dependence on forest above ground biomass since stem volume and biomass are strongly related. Fransson et al. (2000) reports no signs of saturation up to $625 \text{ m}^3 \text{ ha}^{-1}$, and Melon et al. (2001) further extends the non-saturated region to $900 \text{ m}^3 \text{ ha}^{-1}$. The strong dependence between stem volume and HH-polarized VHF-band backscatter is explained by the dominant ground-trunk interaction (Smith, 2000; Smith and Ulander, 2000). That this scattering mechanism dominates also explains the strong dependence on ground slope (Smith et al., 2005; Hallberg, 2007; paper II). In Fransson et al. (2004) a heuristic method for improved stem volume retrieval in sloping terrain is presented. The method requires data from multiple flight paths. In later studies a model based estimation method which includes slope correction is presented and validated (Folkesson, 2008; Folkesson et al., 2008; Folkesson et al., 2009). Using these methods the estimation error in sloping terrain is comparable to that obtained on flat horizontal ground. Results have also indicated the potential of using high resolution VHF band SAR data for estimation of stem volume for individual trees (Hallberg et al., 2005; Kononov and Ka, 2008). The ionosphere affects VHF SAR imaging more strongly than imaging in the UHF-band. However, Belcher (2008) suggests that the lowest usable frequency for a spaceborne SAR might be as low as 100 MHz during favourable circumstances.

Many studies have shown that UHF-band SAR backscatter data are strongly dependent on forest biomass; especially in the low frequency part of the UHF-band (Dobson et al., 1992; Le Toan et al., 1992; Beaudoin et al., 1994). While the sensitivity to forest biomass is generally lower than for VHF band, there is currently no frequency allocation for spaceborne remote sensing in the VHF band. Within the UHF-band several L-band systems have already been launched into space, and a P-band SAR will be realized through the BIOMASS mission (see section 1.4.1). Thus, UHF-band SAR

imaging is a very promising alternative for global biomass mapping. The principles underlying the dependence between biomass and UHF-band SAR backscatter are introduced in the following section. A more extensive treatment is presented in section 4.

1.4 UHF SAR FOR BIOMASS MAPPING

Electromagnetic waves interact most strongly with objects with sizes comparable to the wavelength. The UHF-band comprises wavelengths between 10 cm to 100 cm. Scattering from forests in the UHF-band is therefore dominated by large branches and tree trunks, at least for the longer wavelengths in this band. The large branches and trunks are holders of the majority of the forest biomass. It is therefore reasonable to assume that UHF-band radar images contain information on forest biomass. For shorter wavelengths the scattering originates also from smaller objects in the forest, such as twigs, leaves and needles. These small objects are not significant bearers of biomass, at least not in mature forest. Moreover, the leaves and needles are located near the top of the canopy, since the trees strive to optimize intake of solar radiation. They therefore act to shield the larger branches and trunks from electromagnetic radiation with frequencies above the UHF-band.

In the UHF-band the backscatter from forest is not solely determined by the forest biomass. Surface topography plays an important role, especially for co-polarized scattering (see e.g. paper II). The scattering also depends on dielectric properties of the trunk, branches and ground surface. These properties are in turn strongly dependent on moisture conditions. Another factor which affects scattering is forest structure (Imhoff, 1995a; Smith-Jonforsen et al., 2007). Forest structure is a broad term encompassing tree number density, orientation and size of branches, vertical distribution of woody mass, etc.

Understanding of the complex scattering process can be obtained by physical models. In such models the forest is parameterized and (approximate) solutions to Maxwell's equations are found. Such models are too complex to be directly inverted, but they can give insight on the processes underlying the scattering. A more extensive treatment of this type of physical models is presented in section 4.2. Estimation of forest biomass based on UHF backscatter is often based on empirical models. In such models *in-situ* data are used to derive empirical relationships between SAR data and forest biomass. Empirical models are treated in section 4.3.

1.4.1 THE BIOMASS MISSION

In May 2013 the satellite mission concept BIOMASS was selected to become the European Space Agency's (ESA) seventh Earth Explorer. The BIOMASS concept consists of a SAR operating at 435 MHz (P-band), with a spatial resolution of about 50 m by 50 m (ESA, 2012). The primary objective of the BIOMASS mission is to provide global maps of forest biomass with previously unmatched accuracy and precision. The

mission is considered to be especially valuable in tropical regions, where the current state of knowledge on forest biomass is very poor. BIOMASS will also improve knowledge of boreal and temperate forests, especially in Siberia and China.

Much of the work in this thesis is motivated by the upcoming launch of BIOMASS. Thus, this mission concept plays a central role in the thesis.

1.5 SCOPE OF THIS THESIS

The objective of this thesis is to develop methods for estimating forest biomass and forest biomass change using UHF-band SAR backscatter data, and to evaluate expected errors in these estimates. The main driver for this work was the future P-band SAR mission BIOMASS, but existing and future L-band SAR systems such as ALOS PALSAR (which failed in 2011) also plays a central role. The work in this thesis is confined to boreal and hemiboreal forests. The latter forest biome lies in the transition between boreal and temperate forest. Work has also been done concerning ionospheric distortions, in particular on Faraday rotation. Ionospheric effects are important in the UHF-band. Uncorrected Faraday rotation and other ionospheric distortions can lead to unacceptable quality degradation in UHF SAR images.

The objectives of this thesis are obtained through analysis of data from several data acquisition campaigns conducted in Sweden. These campaigns include the BioSAR 2007, BioSAR 2008 and BioSAR 2010, during which airborne UHF-band SAR data were collected (Hajnsek et al., 2008; Hajnsek et al., 2009; Ulander et al., 2011). The campaigns also include the Calibration and Validation (CalVal) phase of the ALOS PALSAR satellite, during which many L-band SAR images were acquired over an area in which calibration targets were deployed. Since the work in this thesis is based on campaign data its applicability is in a strict sense restricted to these particular data. However, the conclusions drawn in the appended papers also have important implications which are applicable in a broader context.

2 RADAR IMAGING

Radar systems range from fairly simple to extremely complex, and many textbooks devoted to various aspects of radars and their design are available. In this section a brief introduction to radar with focus on radar imaging will be presented. The interested reader can find more thorough descriptions of radar, radar systems and radar imaging in e.g. Carrara et al. (1995), Skolnik (1990), and Sullivan (2004).

2.1 RADAR PRINCIPLES

2.1.1 BASIC SUB-SYSTEMS

Figure 1 shows a block diagram with the basic radar sub systems. In this figure transmission and reception are made with the same antenna (mono-static system). Bi-static systems in which separate antennas are used for transmission and reception are also used.

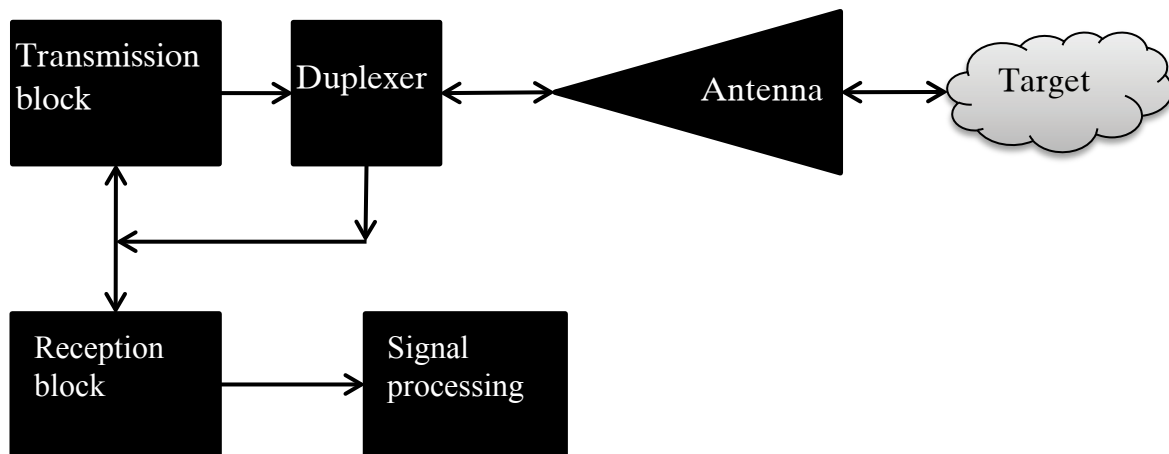


Figure 1. Block diagram showing the main parts of a radar system.

In the transmission block an EM wave with desired waveform and power is generated. The wave is then transferred to the antenna and then into the surrounding medium, most commonly air. The wave is then scattered by some target and received again by the antenna. The duplexer enables transmission and reception using the same antenna by separating the transmit and receive signals from each other. In the reception block circuitry such as low-noise-amplifiers, mixers, various filters and analogue-to-digital converters are applied to the received signal before it is subjected to further signal processing.

2.1.2 RADIOMETRY

The received echo from a target is inevitably corrupted by noise in the receiver. Thus, a very important question is whether or not the echo can be detected in the presence of this noise. This is governed by the radar equation, which gives the Signal-to-Noise-Ratio (SNR) as a function of properties of the radar system, the range to the target and properties of scattering object. The SNR is defined as the ratio between the received

power and the noise power. For a mono-static system using coherent integration during time t_{dwell} it is given by (Sullivan, 2004)

$$\text{SNR} = \frac{P_{avg} \lambda^2 G^2 t_{dwell}}{(4\pi)^3 R^4 k_B T_s C_b L} \sigma \quad (1)$$

P_{avg} is the average transmitted power, λ is the wavelength of the transmitted wave, G is the gain of the antenna, R is the one-way distance (range) to the target, $k_B T_s$ gives the system noise power per unit bandwidth, C_b is a filter mismatch factor and L is a loss factor. Finally, σ is the radar cross section (RCS), with unit m^2 , which is a measure of the scattering strength of a target. A perfectly reflecting sphere has an RCS equal to its cross-sectional area. Thus, the RCS can be thought of as the cross-sectional area of a sphere which gives the same scattered power as the target. For distributed targets it is common to use the backscattering coefficient σ^0 [m^2/m^2]. The backscattering coefficient is defined so that the average RCS from a distributed target with ground area A is $\sigma = A \cdot \sigma^0$.

2.1.3 RANGE RESOLUTION

As explained above, radars measures the electric field induced when the returning echo is received by the antenna. If the speed of light (c) in the medium between target and antenna is known, and it is possible to calibrate for internal time delays of the system, these measurements can be used to measure the range to targets. The resolution in the range direction for radar with bandwidth B is given by (Sullivan, 2004)

$$\delta_R = \frac{c}{2B} \quad (2)$$

2.1.4 PHASE MEASUREMENTS

If the target and/or the antenna move along the range direction, this will cause a change in the signal phase. The rate of change of the phase of a signal is called the Doppler frequency. The non-relativistic Doppler frequency shift is given by (Ulaby et al., 1982)

$$f_D = -\frac{2}{\lambda} \frac{dR}{dt} = -\frac{2v_R}{\lambda} \quad (3)$$

R is the range distance, λ is the wavelength and v_R is the velocity between the target and the radar in the range direction. Pulsed radars generally use too short pulses to be able to measure Doppler shifts within a single pulse. Thus, for pulsed radars the Doppler shift is determined by the change in phase between pulses.

2.1.5 RANGE-DOPPLER AMBIGUITY

For pulsed radars ambiguities can arise for both range and Doppler measurements. If the time between transmitted pulses is too short, an echo originating from a transmitted pulse scattered of a distant object may be received simultaneously as an

echo from a pulse transmitted at a later time scattered from an object closer to the radar. This confusion between range echoes is called range ambiguity. The requirement to avoid range ambiguities places an upper limit on the pulse repetition frequency (PRF). On the other hand, the signal must be sampled with a sampling frequency larger than the range of Doppler frequencies encountered in the signal (Nyquist sampling). Sampling below the Nyquist frequency results in aliasing effects (Doppler ambiguity). For pulsed radars the sampling frequency is the PRF. Thus, if both range and Doppler ambiguities are to be avoided the PRF is constrained both upwards and downwards. Depending on system configurations these requirements can be severe. For spaceborne SAR systems ambiguities place a lower bound on the antenna size, as described in section 2.2.1.

2.2 SAR IMAGE FORMATION

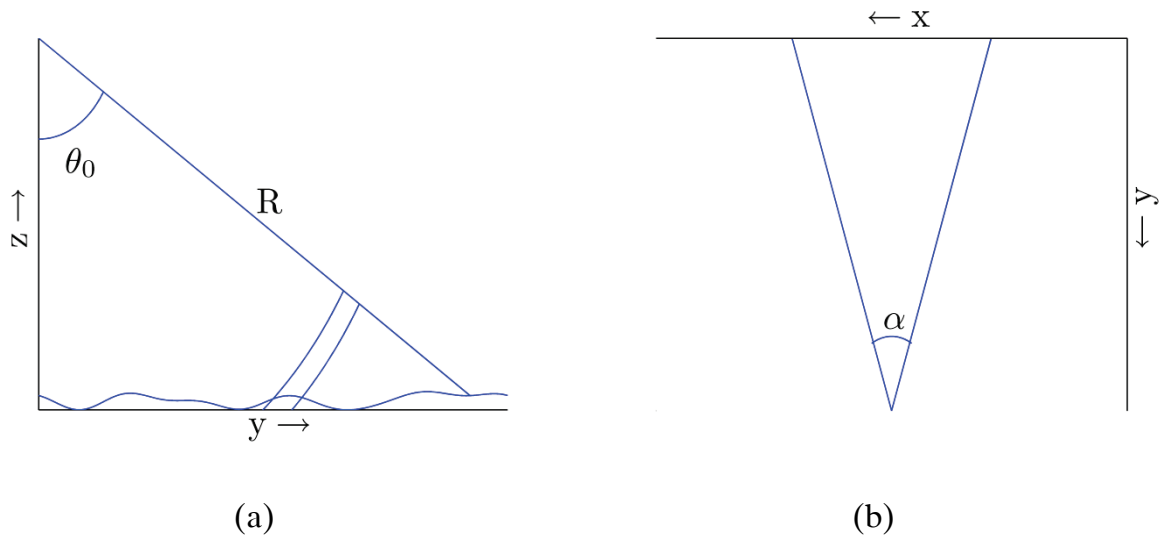


Figure 2. Imaging geometry for a side-looking airborne SAR system. The aircraft travels along the x -axis, θ_0 is the radar look angle and α is the angle over which the target is illuminated.

In remote sensing, as well as many other applications, it is desirable to use radars with imaging capabilities. Imaging enables covering of large areas and is often preferable to line or point measurements. Figure 2 illustrates an imaging geometry for side-looking airborne radar. The coordinate system is right-handed and orthogonal. The aircraft travels along the x -axis, which is commonly denoted the azimuth or along-track direction. The radar transmits pulses perpendicular to the line of flight. The distance between the antenna and a target on the ground is called slant-range distance. The distance along the ground surface is called ground range. The slant range resolution is given by equation 2. To obtain the resolution on the ground surface the slant range resolution cell must be projected onto the ground surface, as indicated in Figure 2.

Without using SAR processing the resolution in the azimuth direction is determined by the antenna footprint. Since this is proportional to the range distance, the resolution becomes poor unless imaging is done at small range distances. However, by using

phase information the azimuth resolution can be significantly improved. There are several viewpoints to aid understanding of the SAR concept. One is to consider that the phase information can be used to create a synthetic aperture much larger than the real antenna. Another viewpoint is that phase information can be used for beam sharpening. After signal processing the azimuth resolution for a narrow beam system is given by (Brown, 1967)

$$\delta_{az} \approx \frac{\lambda}{4 \sin\left(\frac{\alpha}{2}\right)} \approx \frac{\lambda}{2\alpha} \quad (4)$$

Here α is the angle over which the target is illuminated (see Figure 2). The rightmost approximation is valid if $\alpha/2 \ll 1$. From equation 4 it is clear that the azimuth resolution for SAR systems is independent of range distance. If the antenna aperture angle can be approximated by λ/D , where D is the size of the antenna in the along-track direction, and broadside imaging without antenna steering is used, then the azimuth resolution can be approximated by $D/2$. For systems using wide beams and large relative bandwidths the equations for the azimuth resolution are more complex. Moreover, for such systems the resolution cannot be separated into two orthogonal directions. Resolution considerations in ultra-wideband SAR are analysed in e.g. Ulander and Hellsten (1996), Vu et al. (2010) and Vu et al. (2012). For a thorough treatment of SAR image formation and processing see e.g. Carrara et al. (1995).

2.2.1 AMBIGUITY CONSIDERATIONS IN SPACEBORNE SAR

For airborne SAR systems ambiguities are rarely an issue, but for spaceborne SAR ambiguities cause severe constraints on system design. For a given PRF, avoidance of range ambiguities translates to an upper limit on range swath size. This in turn places a lower limit on the size of the antenna in the direction orthogonal to the range direction and to the azimuth direction. The maximum Doppler frequency (assuming stationary targets) is determined by the speed of the spacecraft and the antenna beam width in the azimuth direction. For a given PRF avoidance of Doppler ambiguities therefore translates to a lower limit on the antenna size in the azimuth direction. Combining these constraints place a lower limit on the antenna area. The lower limit is proportional to the wavelength, so that for long wavelengths large antennas are needed. The constraint imposed by range and azimuth ambiguities have the consequence that the swath width and the azimuth resolution cannot be adjusted independently; high azimuth resolution gives a narrow swath, and vice versa. For a detailed discussion on ambiguities in spaceborne SAR see e.g. Ulaby et al. (1982).

2.2.2 INTERFEROMETRY AND TOMOGRAPHY

SAR imaging provides a two dimensional map of the covered area. However, in general the scattering may have a three dimensional structure. To obtain resolution in the vertical direction interferometric or tomographic imaging can be used. The former uses a pair of images. The relative phase between the images in the pair contains

information on the vertical placement of scatterers. This can be used to create elevation maps covering large areas. Interferometry can also be used to track changes in the position of scatterers between image acquisitions. This can be used to detect e.g. landslides. Tomography is a technique for three dimensional imaging. It requires a two dimensional synthetic aperture, which is most commonly obtained by acquiring data from multiple parallel flight lines.

2.3 SPECKLE

Due to their coherent nature, radar images exhibit a property called speckle, which is not seen in normal photographic images. Speckle is a noise-like physical phenomenon which is a property of the image itself and is not caused by any external noise. The origin of speckle can be understood by investigating the received signal from a single resolution cell in a radar image. Invoking the superposition principle, the received signals complex amplitude is the sum of the returns from all individual scatterers within a resolution cell. If the following assumptions hold: a) the phase of an individual scattering object can be assumed to be uniformly distributed, b) there are many scattering objects within the resolution cell, and c) no single scatterer dominates over all others, then the intensity (I) of the received echo has a probability distribution given by (Oliver & Quegan, 2004)

$$p(I|\sigma) = \frac{1}{\sigma} \exp(-I/\sigma), I \geq 0, \quad (5)$$

where σ is the total RCS of the targets within the resolution cell. For this distribution the mean and the standard deviation are both equal to the RCS. Thus, areas with high backscatter will exhibit more variability than areas of low backscatter. It is common to speak of speckle as multiplicative noise, even though at its core speckle is not noise but a consequence of a coherent imaging system.

To reduce speckle in SAR imagery, incoherent averaging must be performed. There are three principal ways to accomplish this. One method is to split the Doppler spectra into several parts, and then forming an image from each of the parts. These different images, often called “looks”, are then averaged incoherently. This process is called “multi-looking”. A second method for incoherent averaging is to average pixels close to each other using a windowing function. A third technique is to average multiple SAR images acquired from the same area at different occasions. This third technique requires that the “true” backscattering coefficient in the area of interest is constant while the speckle changes between image acquisitions. While the term multi-look is most descriptive for the first of these techniques, it is often used for all kinds of incoherent averaging.

The intensity in an image formed by L independent looks has the following probability distribution (Oliver & Quegan, 2004)

$$p(I|\sigma, L) = \frac{1}{\Gamma(L)} \left(\frac{L}{\sigma}\right)^L I^{L-1} \exp(-LI/\sigma), I \geq 0 \quad (6)$$

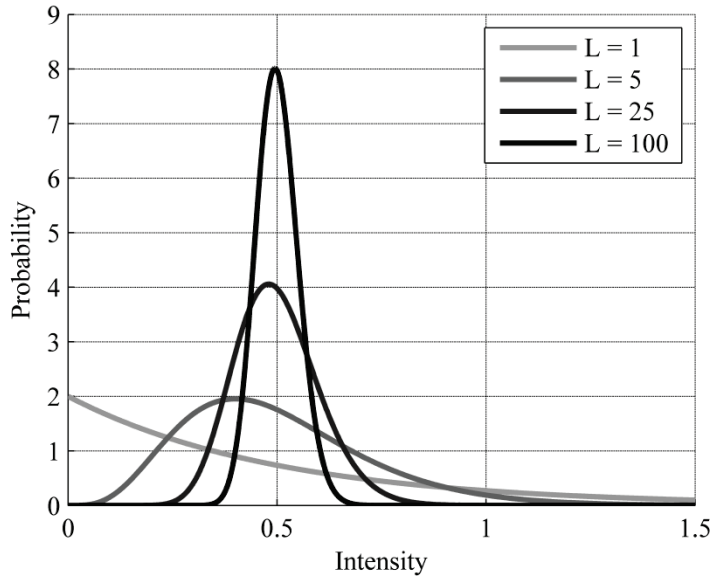


Figure 3. Probability distribution of the intensity in L -look images for different values of L . The mean intensity is 0.5 for all distributions.

In Figure 3 probability distributions of the intensity in L -look images are plotted for different values of L . For low values of L the distribution is highly skewed with long positive tails. For higher L the distribution approaches the normal distribution. The expectation value of an L -look intensity distribution is σ , while the variance is σ^2/L . These properties motivate the definition of an Equivalent Number of Looks (ENL) for a multi-look image. The ENL is defined so that its expectation value for an L -look image is L (Oliver & Quegan, 2004)

$$\text{ENL} = \text{mean}(I)^2 / \text{Var}(I) \quad (7)$$

For real images, the assumptions underlying the speckle distribution are not always valid. In areas with a high degree of texture or with strong scatterers (e.g. cities), the intensity distribution can seldom be approximated by speckle. However, for distributed targets (e.g. forest, fields, and oceans) the speckle approximation often works very well, at least for systems with low or medium resolution.

Important exceptions where the speckle assumptions fail are ultra-wideband VHF and UHF systems. For such systems the resolution can be on the same order as the wavelength. Since targets close to one another (relative to the wavelength) cannot be treated as independent scatterers, the assumptions for speckle cannot be met. An example of a treatment of statistical properties of an ultra-wideband system can be found in Kononov et al. (2011), where images of forests from the Swedish VHF system CARABAS are investigated.

2.4 RADIOMETRIC SAR CALIBRATION

The usefulness of a SAR system is greatly enhanced if it can provide calibrated measurements of RCS (radiometric calibration). Calibrated measurements from different areas and systems can be compared, and stability over time is ensured. Radiometric calibration may be achieved through internal or external calibration, or a combination of the two. External calibration is performed by imaging a target with known RCS, i.e. calibration targets. For internally calibrated systems calibration targets are useful for validation of the radiometric calibration. Both distributed targets and point targets can be used for calibration (Dobson et al., 1986). The latter can be either passive (e.g. corner reflectors) or active (e.g. transponders). Radiometric calibration using point targets can be achieved either by the peak method or the integral method (Dobson et al., 1986; Ulander, 1991a). The latter has the advantage of being independent of system focus, and does not require detailed knowledge of the system impulse response (Gray et al., 1990; Ulander, 1991a; Ulander, 1991b).

For distributed targets, the quantity of interest is the backscattering coefficient (σ^0) rather than the RCS. As stated in section 2.1.2, σ^0 is defined as the average RCS from a distributed target divided by the area of the target on the ground surface. Ulander (1996) presents an analytic method for calibration from RCS in image coordinates to σ^0 in ground coordinates. The method is based on a projection cosine between the image plane normal and the ground surface normal, and is valid when a one-one mapping between ground and image coordinates exists (i.e. excludes layover and shadowing regions). It is shown that this method is superior to the commonly used method based on the local incidence angle in areas with significant azimuth tilts. Methods based on numerical integration of elevation maps may also be used for calibration to σ^0 (e.g. Small et al., (1998)).

2.5 EXAMPLES OF SAR SYSTEMS

In this thesis data from four different airborne systems (CARABAS, LORA, E-SAR and SETHI) and one spaceborne system (ALOS PALSAR) are used, and data from a future spaceborne system (BIOMASS) are simulated. This section presents a summary of the key technical parameters for each of these systems.

2.5.1 CARABAS-II AND LORA

The two ultra-wideband airborne SAR systems CARABAS-II (Hellsten et al., 1996) and LORA (Ulander et al., 2003) were developed by the Swedish Defence Research Agency (FOI). Their initial flight trials were conducted in 1996 and in 2002, respectively. CARABAS-II operates between 20-90 MHz while LORA produces images using the frequency range 200-500 MHz. These two systems are described in more detail in paper II.

2.5.2 E-SAR

The Experimental Synthetic Aperture Radar (E-SAR) is operated by the German Aerospace Centre (DLR) (Horn, 1996). It can operate at P-, L- C- and X-band and is fully polarimetric (experimental polarimetric modes at C- and X-band). It also has capability for polarimetric interferometry. The bandwidth is up to 100 MHz for all frequency bands, giving a range resolution of about 2 m. In azimuth the resolution is specified to 0.7 m (single-look). E-SAR is mounted onboard a Dornier DO228-212 aircraft, and can operate at altitudes up to six kilometres. It delivered its first images in 1988 and has since then been used in numerous remote sensing campaigns throughout the world. Among these campaigns are the BioSAR 2007 and BioSAR 2008 campaigns during which SAR data were collected from Remningstorp in southern Sweden and Krycklan in northern Sweden, respectively (Hajnsek et al., 2008; Hajnsek et al., 2009). Data from these campaigns are used in paper III, IV and V.

2.5.3 SETHI

The SETHI system was developed by the French Aerospace Lab (ONERA). It can operate at frequencies from X-band to the VHF band, and has polarimetric and interferometric capabilities (Angelliaume et al., 2009). The UHF/VHF mode operates from 225 MHz to 460 MHz. The single look resolution in this mode is below one meter in both slant range and azimuth. The SETHI system was used to acquire data for the BioSAR 2010 campaign, during which data were collected from Remningstorp in southern Sweden (Ulander et al., 2011). Data from this campaign are used in paper V.

2.5.4 ALOS PALSAR

On 24 January 2006 the Phased-Array-Type L-band Synthetic Aperture Radar (PALSAR) onboard the Advanced Land Observing Satellite (ALOS) was launched into space (Rosenqvist et al., 2007). ALOS was developed by the Japan Aerospace Exploration Agency (JAXA). Until its failure in 2011 PALSAR provided high-quality L-band images of the globe. PALSAR operated in several imaging modes, including single polarization, dual-polarization, fully polarimetric and scan-SAR modes. The single look resolution in azimuth was 4.5 m and 4.7 m or 9.6 m in slant range, depending on the mode of operation. Scan-SAR modes with coarser resolution were also available. The radiometric, polarimetric and geometric calibration of PALSAR was proven to meet or exceed expectations (Shimada et al., 2009).

2.5.5 BIOMASS

In May 2013 BIOMASS (ESA; 2012) was selected as the European Space Agency's seventh Earth Explorer mission. Its payload consists of a P-band SAR (435 MHz). The bandwidth is limited by ITU regulation to a 6 MHz frequency band (432-438 MHz) allocated for remote sensing (secondary allocation). The bandwidth restricts the slant range resolution to 25 m (single look), resulting in a ground range resolution of about 60 m for an incidence angle of 25 degrees. In the most recent system configuration the azimuth resolution is set to 50 m (six looks).

3 IONOSPHERIC DISTURBANCES

3.1 THE IONOSPHERE

The ionosphere is the outer layer of the Earth's atmosphere. This layer is ionized by solar radiation, and thus contains free electrons. The ionosphere begins at an altitude around 100 km, and the peak electron density is around 250-400 km (Wright et al., 2003). The electron density in the ionosphere can be classified into large scale structures (background ionosphere) and small scale turbulent variations. The large scale structures are determined by largely predictable factors such as local time, season, latitude, and solar activity. The turbulent variations occur on spatial scales from about 10-50 km down to about 2 cm (Belcher, 2008).

A common way to report the electron density is the Total Electron Content (TEC). TEC is the integrated electron density either along a vertical column or along a ray path. The latter is usually called slant TEC (van de Kamp et al., 2009). TEC is often measured in units of 10^{16} electrons per square meter (TECU). Estimates of TEC can be obtained through GPS measurements. On Earth values of TEC are typically 5-100 TECU (Belcher, 2008).

3.2 IMPACT ON SAR OBSERVABLES

When an electromagnetic wave propagates through the ionosphere it interacts with both the free electrons and the Earth's magnetic field. The interaction effects increase in strength as the frequency of the EM wave decreases. Spaceborne SAR images using frequencies in the UHF-band can be affected by the ionosphere in several ways. Image distortion effects include range displacement, range defocus, azimuth displacement, azimuth defocus and Faraday rotation (Bickle and Bates, 1965; Ishimaru et al., 1999; Liu et al., 2003; Wright et al., 2003; Freeman, 2004; Xu et al., 2004; Belcher, 2008; Xu et al., 2008; van de Kamp et al., 2009; Quegan et al., 2012; Rogers et al., 2013). In this section a brief overview of ionospheric effects and methods to correct for these effects is presented. The main focus is on Faraday rotation, which is also the subject of paper I.

3.2.1 BACKGROUND IONOSPHERE

The background ionosphere can be characterized by a mean TEC level and its gradients in the along- and across-track directions. Higher order TEC variations are treated as part of the ionospheric turbulence.

3.2.1.1 RANGE AND AZIMUTH DISTORTIONS

The background ionosphere introduces a frequency dependent phase shift, which may lead to range defocus. However, range defocus is not a strong concern for systems with centre frequency and bandwidth similar to those of BIOMASS or ALOS PALSAR (Belcher, 2008; Quegan et al., 2013). The background ionosphere also causes a

constant phase shift and a range displacement. If range defocus can be neglected these effects are inversely proportional to the centre frequency and the square of the centre frequency, respectively. Both effects are proportional to TEC. TEC gradients in the across-track direction can cause additional distortions across the swath. A constant TEC only cause negligible azimuth distortions. However, TEC gradients in the along-track direction can lead to displacements in azimuth. For a detailed analysis of these effects see e.g. Belcher (2008) and Quegan et al. (2012).

3.2.1.2 FARADAY ROTATION

The refractive index of the ionosphere is birefringent in the UHF-band, with different propagation velocities for left- and right-hand circularly polarized waves. The different propagation velocities cause a phase shift between these two polarization states. For linear polarization this corresponds to a polarization rotation. This effect is known as Faraday rotation. The one-way rotation angle (Ω), given the frequency (f), the strength of the Earth's magnetic field (B), the total electron content and the angles ψ and θ defined in Figure 4, can be approximated by (Wright et al., 2003)

$$\Omega = \frac{K}{f^2} \overline{B \cos \Psi \sec \theta} \cdot \text{TEC} \quad (8)$$

K is a constant with value $2.365 \cdot 10^4 [\text{A} \cdot \text{m}^2 \text{kg}^{-1}]$, and the over-lined expression is calculated at an altitude of 400 km. Two-way travel through the ionosphere results in a rotation twice as large. For a polar orbiting system the factor $\cos \psi$ becomes zero near the equator.

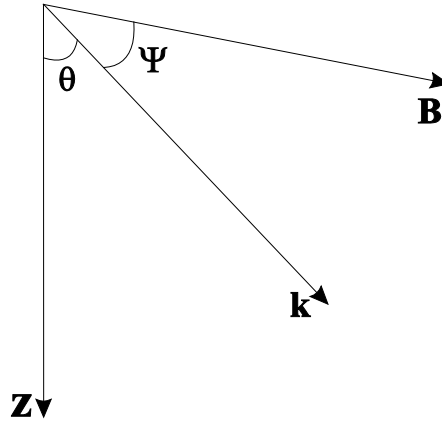


Figure 4. Definition of angles in equation 8. \mathbf{B} , \mathbf{Z} , and, \mathbf{k} are the directions of the Earth's magnetic field, the downward vertical and the propagating EM wave, respectively. The image is reproduced from paper I.

Neglecting a radiometric calibration constant and an overall phase term, the complex valued measurement matrix (\mathbf{M}) for a SAR system transmitting and receiving both horizontal (h) and vertical (v) polarizations can in the presence of system noise

$(N_{hh}, N_{vh}, N_{hv}, N_{vv})$, channel imbalance (f_1, f_2) , cross-talk $(\delta_1, \delta_2, \delta_3, \delta_4)$, and Faraday rotation be expressed as (from Freeman (1992), Freeman (2004), and van Zyl (1990))

$$\begin{aligned} \mathbf{M} &= \begin{pmatrix} M_{hh} & M_{vh} \\ M_{hv} & M_{vv} \end{pmatrix} = \\ &= \begin{pmatrix} 1 & \delta_2 \\ \delta_1 & f_1 \end{pmatrix} \begin{pmatrix} \cos \Omega & \sin \Omega \\ -\sin \Omega & \cos \Omega \end{pmatrix} \begin{pmatrix} S_{hh} & S_{vh} \\ S_{hv} & S_{vv} \end{pmatrix} \begin{pmatrix} \cos \Omega & \sin \Omega \\ -\sin \Omega & \cos \Omega \end{pmatrix} \begin{pmatrix} 1 & \delta_4 \\ \delta_3 & f_2 \end{pmatrix} \quad (9) \\ &\quad + \begin{pmatrix} N_{hh} & N_{vh} \\ N_{hv} & N_{vv} \end{pmatrix} \end{aligned}$$

S_{pq} is the element of the complex values scattering matrix corresponding to polarization $pq, p = h, v, q = h, v$. The rotation matrix is applied both on the downward and upward propagation through the ionosphere.

If system cross-talk, channel imbalance and noise can be neglected and backscatter reciprocity ($S_{hv} = S_{vh}$) is evoked, equation 9 can be expanded to

$$M_{hh} = S_{hh} \cos^2 \Omega - S_{vv} \sin^2 \Omega \quad (10a)$$

$$M_{vh} = S_{hv} + (S_{hh} + S_{vv}) \sin \Omega \cos \Omega \quad (10b)$$

$$M_{hv} = S_{hv} - (S_{hh} + S_{vv}) \sin \Omega \cos \Omega \quad (10c)$$

$$M_{vv} = S_{vv} \cos^2 \Omega - S_{hh} \sin^2 \Omega \quad (10d)$$

From these equations it is clear that when Faraday rotation is present, measurement reciprocity no longer holds. This can be used to estimate the Faraday rotation angle, since there are four complex valued measurements and four parameters (three complex valued and one real) to be estimated. For fully polarimetric data Faraday rotation can be corrected since the rotation matrix is unitary (and therefore invertible). In the presence of uncompensated system calibration effects the estimation problem becomes underdetermined. An overview of correction methods, as well as strategies for compensating calibration effects, is presented in section 3.3.1.

An important note based on equations 10a-d is that Faraday rotation transfers power from the co-polarized to the cross-polarized channels. For small rotation angles this transfer is proportional to the rotation angle. Since for most targets the received power is higher in the HH and VV channels than in the cross-polarized channels, this leakage leads to large distortions of cross-polarized backscatter measurements even for small rotation angles.

3.2.2 SCINTILLATIONS

Ionospheric turbulence can cause phase scintillations across the synthetic aperture. These phase fluctuations can degrade the impulse response function in azimuth, leading to azimuth defocus (Belcher, 2008). Other possible degradations include elevated peak-side-lobe ratios, loss of peak power and image shifts (Rogers et al., 2013). Phase scintillations also degrade interferometric and tomographic image quality.

High frequency GPS estimates of TEC are used in van de Kamp et al. (2009) to study scintillation effects on SAR data. It is concluded that the probability of defocusing for a SAR operating at 435 MHz varies from zero to 45% depending on ionospheric conditions. It is also concluded that the probability of defocus depend strongly on local time and latitude. In Rogers et al. (2013) simulations of scintillation effects on BIOMASS are performed. In this study the wide-band model (WBMOD) is used to obtain climatology data from the strength of turbulence. It is found that the orbit parameters greatly affect the impact of scintillations. It is also found that by choosing a dawn-dusk orbit with an ascending node at 18:00, scintillation “*will have little effect on the ability of BIOMASS to achieve its primary objectives of measuring forest biomass and height, except in the high-latitude North American sector during high solar activity*” (Rogers et al., 2013, section IV). Techniques for corrections of scintillation effects are briefly discussed in section 3.3.2.

Scintillation effects have been observed for the L-band sensor PALSAR. The observed effects are streaks parallel to the magnetic field. Such disturbances have been observed in several PALSAR images with low latitudes (Shimada et al., 2008). These phenomena are studied in detail in Carrano et al. (2012). In this study scintillation effects are simulated for PALSAR images without distortions. Using appropriate parameters for the ionospheric turbulence, the authors are able to reproduce the observed disturbances. These findings confirm that the distortions observed in PALSAR images are caused by scintillation. Note that PALSAR passed over the equatorial region at a local time of about 22:30 on the ascending pass (Rosenqvist et al., 2007), i.e. when ionospheric turbulence is high (van de Kamp et al., 2009; Rogers et al., 2013).

3.3 OVERVIEW OF CORRECTION METHODS

Development of correction methods for ionospheric effects is an essential requirement for successful operation of a P-band satellite SAR. On L-band correction methods for Faraday rotation are needed during high TEC conditions at high latitudes. Moreover, as discussed in the previous section scintillation may also impact L-band SAR data. This section presents correction methods for Faraday rotation and scintillation, with emphasis on the former. Correction methods for other effects, including disturbances of interferometric images, are discussed in e.g. Belcher (2008) and Quegan et al. (2012).

3.3.1 FARADAY ROTATION

ALOS PALSAR created a rise in interest for Faraday correction techniques, and the interest is further enhanced by BIOMASS. Freeman (2004) investigates three methods for Faraday rotation estimation, two new and one proposed by Bickle and Bates (1965). Additional methods are presented by Qi and Jin (2007) (one method) and by Chen and Quegan (2010) (six methods). All of these methods are derived assuming

scattering reciprocity and that system noise as well as system calibration errors can be neglected.

The methods presented by Chen and Quegan (2010) have an ambiguity of π , while the other methods have an ambiguity of $\pi/2$. In e.g. Chen and Quegan (2010) and Quegan et al. (2012) it is proposed that this ambiguity can be resolved by an independent estimate of Faraday rotation based on maps of TEC provided by GPS measurements.

In order to evaluate the performance of different estimation methods several simulation studies have been performed. In Freeman (2004) one of the methods proposed in that paper as well as the method proposed by Bickle and Bates (1965) are evaluated. An evaluation in Meyer and Nicoll (2008) also includes the other method proposed by Freeman. In Quegan et al. (2012) the evaluation is further expanded by including one of the methods proposed by Chen and Quegan. Later in Rogers and Quegan (2013) the method proposed by Qi and Jin is also included. In the two latter studies ambiguity corrections based on TEC maps were included. All of these studies conclude that a) Faraday rotation may be corrected to within the limits required by most applications, and b) the best method for estimation of Faraday rotation is the one presented by Bickle and Bates (1965). This method is based on a transformation of the measurement matrix to a circular basis, after which estimation of Faraday rotation becomes a phase estimation problem. Explicitly, the method is described by the following equations

$$\mathbf{Z} = \begin{pmatrix} Z_{11} & Z_{12} \\ Z_{21} & Z_{22} \end{pmatrix} = \begin{pmatrix} 1 & i \\ i & 1 \end{pmatrix} \begin{pmatrix} M_{hh} & M_{vh} \\ M_{hv} & M_{vv} \end{pmatrix} \begin{pmatrix} 1 & i \\ i & 1 \end{pmatrix} \quad (11)$$

$$\hat{\Omega} = \frac{1}{4} \arg(\langle Z_{12} Z_{21}^* \rangle) \quad (12)$$

As is clear from the papers discussed above, Faraday rotation can be corrected for fully polarimetric UHF-band SAR data. Note that this conclusion only is valid for fully polarimetric systems. By using circular polarizations it is possible to obtain measurements undistorted by Faraday rotation without measuring the full scattering matrix. However, circular polarizations have been proven to be less sensitive than linear polarizations to physical variables such as forest biomass (Rignot et al., 1995).

3.3.2 SCINTILLATION

Scintillations may potentially have an impact on the quality of UHF-band SAR images, and are discussed in e.g. Belcher (2008), van de Kamp et al. (2009), Quegan et al. (2012) and Rogers et al. (2013). As discussed above the most severe effect of scintillations is defocusing in azimuth. In Belcher (2008) along-track autofocus is discussed as an option for correcting defocus caused by scintillations. However, it is noted that high signal-to-clutter ratios are required to obtain reliable results. Thus, autofocus techniques are not suitable for homogeneous areas. In Quegan et al. (2012)

an alternative method for correction method is proposed. This method is based on the following observations:

- a) Defocus is caused by small scale variations in TEC.
- b) It is possible to measure Faraday rotation with low errors and at high (kilometre scale) resolution using fully polarimetric P-band SAR data.
- c) Estimates of Faraday rotation can be used to obtain a map of TEC at spatial scales dominated by scintillations.

The TEC map based on Faraday rotation estimates can then be used to correct scintillation effects. The method produces promising results, but requires further study before definite conclusions on its validity can be drawn.

3.4 SUMMARY OF PAPER I

The objectives of paper I were two-fold. The first objective was to assess residual system calibration errors of the ALOS PALSAR system, in particular system cross-talk and channel imbalance. The other objective was to provide validated estimates of Faraday rotation in PALSAR images. To these ends, fully polarimetric PALSAR data from the test site Remningstorp in southern Sweden were used. In this site trihedral reflectors were deployed (see Figure 5), providing reference targets with high signal to clutter ratios (SCR). Data for this study were collected between 20 May 2006 and 4 December 2006, partly within the Calibration and Validation (CalVal) phase of PALSAR. Eight images, four acquired on the ascending and four on the descending pass, were used. These images were calibrated by JAXA. Maps of TEC from the International Global Navigation Satellite System Service were also used. These maps had a reported root mean squared error (rmse) of less than 0.7 TECU.

As a first step residual cross-talk levels were estimated during conditions of low ionospheric electron content (two images for which the TEC was below 3 TECU). Under these conditions Faraday rotation was considered to be negligible, and residual cross-talk levels were estimated. The cross-talk was found to be below -35 dB, strongly indicating that PALSAR was a well isolated system.

Under the assumption that system cross-talk could be neglected, Faraday rotation and channel imbalance were estimated for each of the eight PALSAR images. To estimate both these quantities simultaneously reflector responses were used. Moreover, the response from an area for which it was assumed that the co- and cross-polarized channels were uncorrelated was also used. Faraday rotation angles were estimated using two methods. The first method was proposed by Bickle and Bates (1965) (see section 3.3.1), while the other method was based on reflector responses.



Figure 5. One of the corner reflectors in the process of being adjusted for a ALOS PALSAR image acquisition. The image can also be found in paper I.

The balance between channels was found to be good. Faraday rotation angles up to 3 degrees were estimated. The two methods for estimation of Faraday rotation showed very good agreement. Moreover, estimated Faraday rotation angles showed good correlation with TEC, giving further evidence of the validity of the estimates.

In summary, paper I concludes that PALSAR was well isolated with low channel imbalance. It also shows that Faraday rotation can be measured in PALSAR data using both the method proposed in Bickle and Bates (1965) and the method based on reflector responses.

3.5 CONCLUSIONS AND OUTLOOK

As discussed in this section the ionosphere can have a large impact on SAR observables in the UHF-band. However, it is clear that by minimizing ionospheric disturbances (e.g. selection of orbit parameters) and by utilizing correction techniques, this impact can be mitigated. As an example, it is shown in Quegan et al. (2012) that ionospheric disturbances do not pose a threat for the fulfilment of the primary objectives of BIOMASS.

The importance of ionospheric mitigation techniques is made clear by the ionospheric effects observed for PALSAR. Faraday rotation has been observed in many PALSAR images. Although these angles are often small enough to be neglected, large Faraday rotation angles can be present in L-band images (Wright et al., 2003). Scintillations

effects observed for PALSAR imagery further stress the importance of mitigation techniques (Carrano et al., 2012).

While correction techniques for Faraday rotation are well investigated, correction schemes for other effects are less mature. Most notable is corrections for ionospheric scintillations. Interesting results are presented in Quegan et al. (2012), but further studies are needed. With successful correction techniques it might be possible to obtain high quality P-band data also at high latitudes.

4 UHF SAR FOR BIOMASS MAPPING

Over the past decades several studies have illustrated that UHF SAR backscatter show a strong dependence on forest biomass (see e.g. Le Toan et al. (1992), Dobson et al. (1992), Beaudoin et al. (1994), Israelsson et al. (1994), Israelsson, (1998), Fransson (1999), and Saatchi et al. (2007)). Investigations of UHF-band scattering from forests are the primary objective of this thesis. A key to understanding the scattering from forests are physical scattering models. A scattering model valid for HH-polarized data in the VHF band and the lower part of the UHF-band is presented in paper II. In paper III and paper IV the possibility to estimate biomass using UHF-band backscatter is analysed. In paper V methods for estimation of forest biomass change using P-band SAR data are developed and analysed.

This section is organized as follows. First a general discussion of parameters contributing to UHF-band scattering is presented. Then a brief overview of physical scattering models is presented, including a summary of paper II. In the following section empirical models for estimation of forest biomass based on UHF-band backscatter are discussed. Important considerations regarding empirical regression modelling are presented, followed by an overview of studies using this approach to biomass estimation. Paper III and paper IV are also summarized, and general conclusions are discussed. After this the focus is shifted to biomass change measurements, and paper V is summarized. Finally, some general conclusions concerning biomass estimation using UHF-band backscatter are drawn.

4.1 WHAT AFFECTS THE SCATTERING?

It is often useful to divide the scattering from forests into different scattering mechanisms. Figure 6 illustrates the main scattering mechanisms for UHF-band. These are direct scattering from the ground, canopy (branches and leaves/needles) and trunk. Scattering from the ground-trunk and ground-canopy interactions are also included in the figure. Note that, due to reciprocity, these mechanisms will add in-phase with their reciprocal mechanisms (i.e. trunk-ground and canopy-ground interactions). Higher order multiple scattering such as branch-branch or ground-trunk-ground interactions may also be considered. An important note is that the separation of the total scattering into scattering mechanisms is an approximation in which near-field interactions between scatterers are neglected.

Forests are complex targets which cannot be fully characterized by a single parameter. Thus, the backscatter from forests in the UHF-band is not only determined by the forest biomass. One important parameter is the ground topography. For HH-polarized backscatter the trunk-ground interaction play a significant role, at least for P-band (paper II). Recent results based on tomography also indicate that ground-canopy or ground-trunk interactions are important for cross-polarized P-band backscatter (Tebaldini and Rocca, 2012).

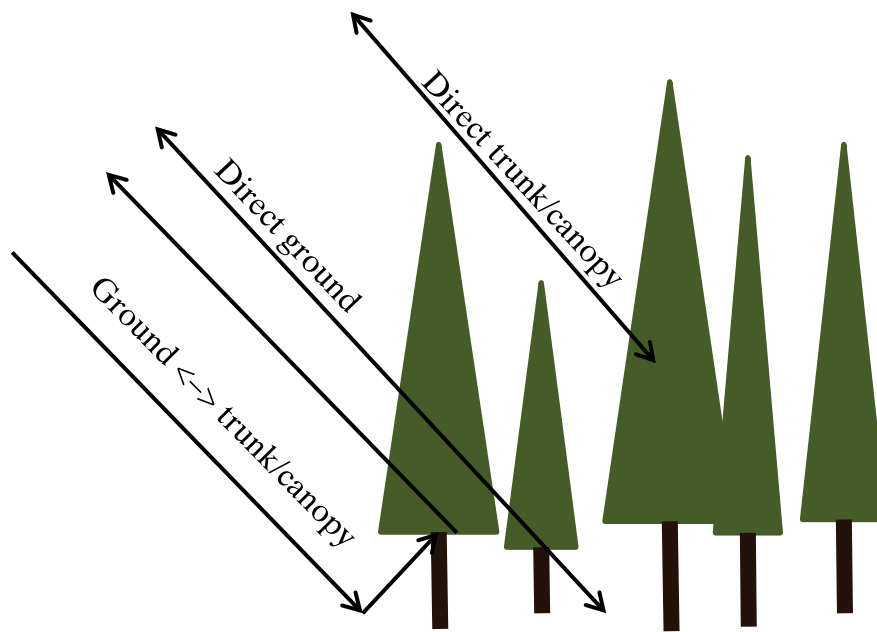


Figure 6. Main scattering mechanisms for UHF-band scattering from forests.

Scattering from ground surfaces depends on small- and large scale topographic undulations, as well as on the dielectric properties of the surface (Ulaby et al., 1982). The dielectric properties are in turn strongly affected by the moisture content. When the trunk-ground interaction is important both large scale slopes and small scale undulations play a significant role (paper II; Smith-Jonforsen et al., 2005). The dielectric properties of the forest itself also affect the backscatter. For wood the dielectric constant is mainly determined by the moisture content and the wood density (Torgovnikov, 1993). Since scattering from both the trees and the ground are influenced by moisture content, moisture variations affect the scattering strength leading to seasonal and environmental variability (Santoro et al., 2009).

Another important parameter is forest structure, which has been shown to have an impact on scattering strength (Imhoff, 1995a; Smith-Jonforsen et al., 2007; Folkesson, 2008). The structure of the forest can be defined as the vertical and horizontal distribution of woody material within a forest. Examples of parameters contributing to forests structure are tree species, tree number density, and undergrowth. Forests with similar biomass but different structure, e.g. many small trees or a few large trees, can give rise to different backscatter levels. In managed forests the structure is to a large part determined by management practices such as thinning and plantation. The resulting constraints on structure diversity may contribute towards simple relationships between UHF backscatter and forest biomass (Imhoff, 1995a). The effects of the more complex forest structure in e.g. tropical rainforests are difficult to predict. However,

results based on airborne data from tropical rainforests in French Guiana indicate that P-band backscatter can be used to estimate forest biomass with estimation errors in the order of 20-25% of the mean biomass (ESA, 2012).

4.2 PHYSICAL FOREST SCATTERING MODELS

Physical models for prediction of scattering from forests are important tools for gaining deeper understanding of the processes underlying the scattering. This type of models can be divided into two categories: models based on wave theory and models based on energy transport (radiative transfer) (Saatchi and McDonald, 1997). These two categories can also be labelled coherent and incoherent modelling.

In models based on wave theory the starting point is Maxwell's equations. In principle a complete numerical solution can be calculated, but the complex scattering geometries in forests make this approach unfeasible except in simplified cases. To decrease the computational burden the forest is assumed to consist of a set of scattering objects (e.g. trunks, branches, ground), and near-field interactions between scatterers are neglected. Moreover, far-field interactions between scatterers (multiple-scattering) are often completely or partially neglected. The trunks, branches, leaves and needles are modelled as a set of dielectric cylinders and discs, for which approximate solutions to Maxwell's equation exists. This approach has been used to model trunks on flat or sloping terrain (Dong and Richards, 1995; Lin and Sarabandi, 1995; Lopez-Sanchez et al., 1999) as well as more general forests structures including trunks and canopy (Lin and Sarabandi, 1999; Thirion et al., 2006). In paper II, HH-polarized scattering from vertical trunks above an undulating ground surface is modelled for VHF and UHF-band.

For models based on energy transport the starting point is propagation of energy instead of waves. The equations which govern energy transport are called radiative transfer equations. This is a simpler approach than wave theory models, which is a benefit especially in analytical treatments. Multiple scattering may be modelled by including high-order solutions of the radiative transfer equations. Studies adopting this modelling approach include Hsu et al. (1994), Imhoff (1995a), Karam et al. (1992), Liang et al. (2005), Picard et al. (2004), and Ulaby et al. (1990).

Although different models vary in details, most studies agree that P-band backscatter is more strongly related to biomass than L-band backscatter. Moreover, most studies agree that HV-polarized backscatter shows better sensitivity to forest biomass than other polarizations. Most models also conclude that the backscatter for HV is dominated by direct scattering from the branches, although in Israelsson et al. (1994) results from a radiative transfer model indicate that ground-canopy scattering is important for P-band HV data. The models tend to agree that P-band VV-polarized backscatter is not dominated by a single scattering mechanism, and that VV-polarized backscatter shows the least sensitivity to biomass. For HH-polarized backscatter model results are less conclusive, as discussed in paper II. Some studies indicate that the

ground-trunk interaction is dominant, at least in the low-UHF-band, while other results support the conclusion that branch scattering is important. Part of the explanation for these discrepancies is that the model results are sensitive to changes in input parameters such as branch angle and branch radius (Hsu et al., 1994). The results in paper II indicate that for spruce-dominated forest in flat terrain the scattering behaviour is well characterized by the ground-trunk interaction if undulations of the ground surface are included in the model.

4.2.1 SUMMARY OF PAPER II

Paper II presents a model for prediction of HH-polarized backscatter from coniferous forest in the VHF and (lower) UHF-bands¹. The model is based on a physical-optics approach. The ground is modelled as an undulating surface described by a set of surface facets, and the trees are modelled as vertical trunks (tapered cylinders). The model was validated against data from the airborne SAR systems CARABAS and LORA. Detailed *in-situ* measurements were used to specify the diameters and heights of the trunks, and the ground surface was adjusted to match measurements from high-density laser scanning data. It was found that the model was able to predict much of the variation in the backscatter, giving coefficients of determination of 0.44 and 0.65 for VHF and UHF frequencies, respectively. When using the same model with a flat ground surface the coefficient of determination dropped to about 0.1. These results indicate that undulations in ground topography on scales similar to the wavelength are an important effect in HH-polarized VHF and UHF SAR imagery. The model was not able to predict the absolute values of the backscatter, which is believed to be explained by the chosen value for the stem dielectric constant, as well as un-modelled effects such as wave attenuation, small scale roughness and tilting stems.

4.3 EMPIRICAL ESTIMATION MODELS

As described in the previous section physical models for prediction of backscatter from forests are extremely complex and rich in parameters. This complexity is a natural consequence of the nature of UHF scattering from forests. For these frequencies the scattering originates from both trunks and branches, and the interaction with the ground surface can in most cases not be neglected. Branches vary in size, shape and orientation between different species as well as between individual trees. Moreover, at these frequencies the ground is not easily characterised with few parameters (paper II).

¹ Note that paper II used the definition of UHF-band common in the radar community, i.e. 300 MHz to 1000 MHz. In the rest of this thesis the ITU definition of UHF to include frequencies between 300 MHz and 3000 MHz is used.

Since the number of parameters in physical scattering models is far greater than the number of measurements provided by SAR data, it is unfeasible to invert such physical scattering models to estimate biomass. An alternative approach is to collect both SAR data and reference forestry data from one or several test sites, and then use regression analysis to derive a relationship between SAR measurements and forest variables.

4.3.1 EMPIRICAL AND SEMI-EMPIRICAL MODELS

There are two different types of models which can be used in regression modelling. One option is to use simplified physical reasoning to determine a functional form for the regression model. Some, or all, of the parameters for this model are then determined from an (often non-linear) regression analysis. Such models are often called semi-empirical, to reflect the fact that they are a combination of physical modelling and empirical observations. In the other kind of regression model both the functional form of the model and the values for the parameters are inferred from the data itself. In the following such models will be referred to as empirical models.

There are several examples of semi-empirical models which have proved to be successful. One example is the description of scattering from sea surfaces by using Geophysical Model Functions (GMFs) (Long, 1995; Stoffelen, 1998). Several variants of GMFs are used operationally to estimate wind speed over the Earth's oceans with scatterometry and SAR data (Hersbach et al., 2007; Quilfen et al., 1998; Stoffelen, 1998). Another example of a successful semi-empirical model is found in Folkesson et al. (2009). Here a simplified physical model for scattering from forest in sloping terrain at the VHF band is presented and analysed. It is shown that with this model it is possible to obtain similar estimation errors for sloping terrain as for flat ground.

Semi-empirical models for backscatter from forests are by nature forward models, i.e. they aim to predict the backscatter based on forest properties. Empirical models do not have this inherent limitation. To obtain forest properties given a forward model and a set of measurements, the model needs to be inverted. This may be a straightforward task, but a disadvantage with semi-empirical modelling is that the inversion process may be difficult. This problem is discussed in Fransson and Israelsson (1999), where the relation between ERS-1 and JERS-1 backscatter and forest stem volume is analysed. A semi-empirical model called the water-cloud model (Attema and Ulaby, 1978) is used to predict backscatter from forest given the stem volume. The water-cloud model is found to be successful at this task. However, the authors found that this model was "*unsuitable for developing a radar-based model of stem volume*" (Fransson and Israelsson, 1999, p. 133). They instead used an empirical model to estimate stem volume from radar backscatter. Thus, if the primary goal is to estimate forest variables with low error, semi-empirical modelling might not be the best choice.

A risk with semi-empirical models is that oversimplified physical modelling may lead to erroneous physical interpretations. To illustrate this point, consider the following

example. A simple semi-empirical model aims to describe backscatter from a forest using a function on the form

$$\sigma^0 = f(W|\theta) + b(W) + \epsilon(W). \quad (13)$$

In the equation above σ^0 is the backscattering coefficient, W is the forest biomass, $b(W)$ is a modelling bias, $\epsilon(W)$ is a random error with zero mean, and θ are model parameters. Now, in a semi-empirical model the parameters θ have some physical interpretation under the modelling assumptions. However, if the modelling error (bias and random error) is large, estimates of θ may be dominated by the error. This may in turn lead to misleading physical interpretations of the fitted model.

There are of course disadvantages to empirical models as well. Perhaps the strongest objection is that the lack of physical modelling increases the risk of adapting the empirical model too strongly to a particular dataset. With a semi-empirical model the functional form of the model is given, and there are often physical constraints on the parameters. Empirical models do not have such constraints, which may result in models for different dataset which are very different from one another. Thus, it is very important to be careful when developing empirical models.

One important consideration in empirical modelling is to make sure that the model does not lead to strange physical interpretations. A trivial example might be a model which predicts that long men weigh less than short ones. Such a model might arise from “blind” regression modelling using a small dataset which only includes adults with very similar weight, and includes individuals which are very long and thin. Another important consideration is to compare new empirical models to similar models which already exist. This will help to ensure that results from various datasets are consistent. Consistency of course do not imply correctness, but if a new model deviate strongly from other published models this must be analysed and discussed.

Empirical models should be developed in a way which is statistically sound and well-motivated. This aspect of empirical modelling is the topic of the following section.

4.3.2 MODEL SELECTION AND EVALUATION

When developing an empirical model, it is important to realize what the purpose of this model development is. Most often the goal is to develop a model to be used for prediction, i.e. to estimate a physical variable (e.g. biomass) given a set of measurements (e.g. backscatter measurements). In the following the variable to be estimated will be referred to as the response variable, and the measurements will be called predictor variables or simply predictors. It is important to realize that prediction is often performed on *new* data with similar properties as the data used for model development. Thus, the question is not which model that best describes the data, but rather which model that can be expected to give the lowest estimation error for new data. Moreover, it is also important to estimate how large this estimation error can be

expected to be. This section provides an overview of common methods that can be used to select and evaluate the “best” model among a set of candidate models.

Empirical models vary in complexity. On one end there are very complex models such as local averaging methods. On the other end there are simple linear models, where the relation between the response and predictor variables is a simple linear function with known properties. In this section the focus is on linear models, but much of the ideas presented here can be generalized to more complex models. Moreover, by using transformations of the response and predictor variables, as well as higher order power function of the predictor variables, complex functional relationships can be created within the bounds of linear models.

A linear regression model can be described as

$$y = f(\mathbf{x}|\boldsymbol{\beta}) + \epsilon = \beta_0 + \beta_1 x_1 + \dots + \beta_p x_p + \epsilon \quad (14)$$

y is the response variable, $\mathbf{x} = (x_1, x_2, \dots, x_p)$ are the predictor variables, $\boldsymbol{\beta} = (\beta_0, \dots, \beta_p)$ are the regression coefficients and ϵ is a random error. Linear models are discussed in detail in e.g. Rawlings et al. (1998). The regression coefficients for a standard linear model are usually estimated using least squares. This estimation method relies on some model assumptions, which are discussed below. While these are basic material in any regression book or course, they are essential when developing regression models and deserve to be discussed here. Moreover, the process of evaluating these assumptions often leads to a better understanding of the dataset that is the basis for the estimation problem.

4.3.2.1 ASSUMPTIONS IN LINEAR REGRESSION

First, it is assumed that the linear model is sufficient to describe the data. This assumption might be violated if for instance an important predictor variable has been omitted from the model, or if a quadratic dependence on a predictor variable is modelled as a first power relationship. An inadequate model leads to biased estimates of both prediction errors and regression coefficients. The most important tool for spotting inadequacies in a model is by plotting the data. There are many kinds of diagnostics plots, see Rawlings et al. (1998) for details. Visualizing the data by plotting and close study of diagnostic plots is essential in statistical model development. Other ways to detect model inadequacies include previous experience with similar datasets, as well as theoretical knowledge (e.g. physical reasoning and modelling).

Further assumptions are that the error variance is constant and that the errors are symmetrically distributed (since the square of the error is used to measure dispersion). These assumptions are most easily checked using diagnostic plots. For some inference analysis the errors are also assumed to be normally distributed, but moderate deviations from normality can often be tolerated (Rawlings et al., 1998). Violations of these assumptions primarily leads to erroneous estimates of dispersion

(e.g. estimation errors), but also results in ineffective and possibly biased estimates of regression coefficients. If possible, violations of these assumptions can be remedied using variable transformations. Another option is to use weighted and/or non-linear least squares (Rawlings et al., 1998).

Another assumption is that all residuals in the data are uncorrelated. Correlation structures can be spotted by careful consideration of how the data was collected. For example, data groupings (e.g. data from different test sites) and time sequences are causes for concern. Correlations structures in the data lead to loss in precision in estimates, as well as serious bias in measures of dispersion. Solutions to these problems include time-series analysis, mixed effects models and generalized least squares (Rawlings et al., 1998).

If an observation, or a group of observations, deviate from the rest in one or several of the predictor variables, this observation will have a strong impact on the regression analysis. This is an undesired effect, since the results will be greatly affected by just a few observations. Observations may also deviate in the value of the response variable. Such observations can often have large residuals, which may lead to an overestimation of the model error since least squares give large relative weight to large residuals. Deviating observations (outliers) must be treated with care. A good option is often to do the analysis both with and without the outlier in order to investigate its impact. However, an outlier should never be excluded from the analysis without careful discussion of the reasons for this exclusion.

4.3.2.2 MODEL SELECTION

Model selection is, in this context, the process of selecting the model(s) best suited for prediction of the response variable. For linear models, model selection simplifies to the process of selecting which of the predictor variables to include in the model. It should be noted that in the following it is assumed that the basic model assumptions discussed above are valid. Checks of model assumptions are often an iterative process; as new models are developed the assumptions need to be rechecked.

Model selection techniques can be divided into two broad categories. One category relies on penalization of large models or pairwise model comparisons. Methods based on penalization include Mallows' C_p (Mallows, 1973), the Akaike information criterion (AIC) (Akaike, 1969), the Bayesian information criterion (BIC) (Schwartz, 1978), and many variations thereof. Common methods based on pairwise model comparisons are forward selection, backward elimination and stepwise regression (Rawlings et al., 1998). The other category of model selection methods is based on data resampling or data splitting, and include bootstrap and cross-validation methods (see e.g. Arlot and Celisse (2010), Breiman and Spector (1992), Picard and Cook (1984), Shao (1993), and Zhang (1993)).

An attempt to judge which of the wide variety of model selection methods that is the “best” is far beyond the scope of this thesis. It is sufficient to say that this issue has been, and still is, a topic of discussion. One issue in this discussion is that there are several ways to define “best”. Note also that none of the selection models can be used blindly on a dataset, care must always be taken to ensure that model assumptions are valid (see above) and that the final model is reasonable from a scientific point of view.

Moreover, the goal of model selection is often not to pick a single model and claim that this is superior to all others. Instead the most common scenario is that there are a few, or many, models which give similar estimation performance, and judging which of these that is “best” is often not possible. This ambiguity should be made clear, even if only one model is selected. An alternative approach is to select several models and compare their results. Yet another option is to use the average of several models when using predictions. This option is discussed in e.g. Hoeting et al. (1999).

4.3.2.3 MEASURES OF GOODNESS OF FIT AND PREDICTION PERFORMANCE

As is clear from the discussions above, the primary goal of empirical modelling in this context is prediction. Thus, it is essential to provide an estimate of the expected prediction error. A common measure of prediction error is the mean squared error of prediction (MSEP), defined as the average squared difference between independent observations and predictions corresponding to these observations (Rawlings et al., 1998). The most straightforward way to obtain an estimate of MSEP is by applying the developed model on an independent dataset (validation). An objection to reserving data for validation is that this process decreases the size of the training data, which results in larger uncertainties in estimated model parameters. This may in turn lead to uncertain error estimates. This issue motivates resampling methods such as cross-validation and bootstrap. It is important to stress that the residual error, i.e. the error obtained for the training data, almost always underestimates the prediction error (Rawlings et al., 1998). Thus, the residual error should not be used as an estimate of prediction performance.

A note of caution is that large errors may occur if estimation models are used for data different from that used for training. For example, an estimation model for biomass developed for boreal conditions should not be used in tropical forests. Determination of the proper validity range for models predicting forest variables from remote sensing data is a difficult task, which requires data from more than one test site (see e.g. paper IV).

A commonly used quantity for measuring goodness of fit is the coefficient of determination (R^2), usually given in percentage units. There exist several different expressions for R^2 , many of which are equivalent in the context of linear regression with an intercept term (i.e. β_0 in equation 14) included in the model. In Kvålseth (1985) the following expression for R^2 is recommended

$$R^2 = 1 - \frac{\sum(y - \hat{y})^2}{\sum(y - \bar{y})^2} \quad (15)$$

Here y is the variable to be estimated, \hat{y} are estimates of y and \bar{y} is the mean value of y . The commonly used interpretation for R^2 is that it indicates how large part of the variation in the response variable that is explained by the predictor variables (Rawlings et al., 1998). A note of caution is that R^2 can be inflated by single observations with predictor values which deviate from those of other observations.

4.3.3 OVERVIEW OF REGRESSION BASED STUDIES

There are many studies in which the relation between UHF-band SAR data and forest biomass has been investigated. Many of these studies are based on data from the airborne sensor AIRSAR, which was developed by the National Aeronautics and Space Administration (NASA) and the Jet Propulsion Laboratory (JPL) in the late 1980s. Later studies have used data from the airborne sensors E-SAR and/or SETHI, which provide SAR images with better resolution than AIRSAR. In this section an overview of studies on the relation between UHF data and forest biomass is presented. Only studies which include P-band data are presented. Thus, studies based solely on spaceborne sensors (e.g. JERS-1 and ALOS PALSAR) are not included.

In Le Toan et al. (1992) and Beaudoin et al. (1994), AIRSAR data collected from the Landes forest in south-western France are investigated with respect to its dependence on forest biomass. This is a plantation forest completely dominated by maritime pine, and consists of large homogeneous forest stands in flat terrain. In a preliminary assessment the biomass estimation error is estimated to be about 20%.

AIRSAR data from the Landes forest are pooled with ARISAR data from Duke University Research Forest in North Carolina in Dobson et al. (1992). Both sites contain even-aged stands of pine trees. For L- and P-band backscatter the data from the two sites have a similar dependence on biomass, and no clear systematic differences between the two sites are observed.

Data from a test site near Howland, Maine were analysed in Ranson and Sun (1994). The test site lie on the border between coniferous boreal forest to the north and hardwood forest to the south, and consist of mixtures of e.g. hemlock, spruce, fir and hardwood (aspen, birch, maple, and beech). The biomass reaches 370 t/ha, with gently rolling topography. SAR data from AIRSAR were used to develop regression models for biomass estimation. L- and P-band HV data were used in the analysis, as well as the ratios between these polarizations and C-band HV. Coefficients of determination of 0.75 and 0.81 were reported when using L-HV and P-HV, respectively. A multi-temporal analysis was also performed. This analysis indicated that the regression model developed using data from 1991 could be applied to SAR data from 1989. The data used by Ranson and Sun (1994) are further analysed in Ranson and Sun (1997). A radiative transfer model described in Sun et al. (1991) was used together with a model

simulating forest dynamics to obtain a database of simulated radar responses for a wide set of forest conditions. The simulated data were then used to develop regression models for biomass prediction. Only co-polarized simulated data were used. Using a ratio between P-HH and C-HH the model derived from simulated data gave an rmse of about 65 t/ha, similar to the error obtained from a similar model developed using experimental data. When using HV data the rmse decreased to about 50 t/ha. Lower errors were found when the maximum biomass was reduced from 370 t/ha to 150 t/ha.

In Rauste et al. (1994) AIRSAR data collected from a test site close to Freiburg in south-western Germany were used to estimate stem volume, which can be used as a proxy for biomass. Note, however, that the conversion from stem volume to biomass depends on e.g. species and age (see paper III). The test site is dominated by coniferous temperate forests with stem volumes ranging up to $800 \text{ m}^3\text{ha}^{-1}$ (about 500 t/ha). Inventory data were available for 230 forests stands, although the inventory predated the AIRSAR data collection by nine years. The stands were divided into a training set used for model development and a validation set used to estimate the prediction errors. Using P-band HV the error was estimated to between $140 \text{ m}^3\text{ha}^{-1}$ and $170 \text{ m}^3\text{ha}^{-1}$ (about 85 t/ha to 100 t/ha). The authors list the following reasons for why these errors are higher than in similar studies: a) the nine year separation between the *in-situ* inventory and SAR data acquisition makes the inventory data unreliable b) the test site shows strong topographic variability and large species diversity compared to other sites, and c) the maximum biomass level is higher than in other sites.

In Rignot et al. (1995) the possibility to estimate biomass from P-band SAR data is evaluated for four test sites. The sites are Landes forest in France (temperate forest), Duke University Forest in North Carolina (temperate forest), Bonanza Creek experimental forest in Alaska (boreal forest), and finally Manu National park in Peru (tropical rainforest). Data from the first and third of these sites were also analysed in Rignot et al (1994). Using HV, HH as well as the ratio between HH and VV backscatter as predictors, error rates are found to be 14% for Landes forest and about 30% for Duke University Forest and Bonanza Creek experimental forest. Note that these errors are based on mean absolute error rather than the more commonly used root mean squared error. For the tropical site the authors state that the sample plot areas are too small for a quantitative error evaluation. In Rignot et al. (1994) an evaluation of L-band data from Bonanza Creek experimental forest is also included. The estimation errors based on L-band data are similar to or slightly worse than those based on P-band data for this dataset.

In Baker et al. (1994) SAR data from the Thetford forest, UK, acquired using AIRSAR, are analysed and used to estimate timber volume. This test site is a managed productive forest with even-aged stands dominated by pine. Timber volumes up to $500 \text{ m}^3\text{ha}^{-1}$ were present within the site, which according to the authors corresponds to about 185 t/ha. It is concluded that timber volume can be estimated with an error of about 20% using P-band HV backscatter.

AIRSAR data from two coniferous (Landes, France and Duke University Forest, North Carolina) and one broadleaf evergreen (Volcanoes National Park, Hawaii) test sites were analysed in Imhoff (1995b). In this study saturation levels, i.e. biomass levels above which SAR backscatter has reduced sensitivity to biomass, are determined. Saturation levels are obtained both by fitting of ninth-order polynomials and by visual inspection. Saturation levels are determined to be about 40 t/ha and 100 t/ha for L- and P-band, respectively. A note in this context is that recent results have demonstrated that P-band backscatter may be used to estimate biomass above these saturation limits (ESA, 2012, see also paper III and paper IV).

In Hoekman and Quiriones (2000) AIRSAR data from the Guaviare district in Columbia were analysed. The imaged area covers both the Amazon rainforest and savannahs, but the focus of the study is on the former. Deforestation and land cover change are common in this area. A classification scheme based on multi-frequency and multi-polarized data is used to classify the area into four land-cover types: primary forest, secondary forest regrowth, recently burnt forest and pastures. Classification accuracies of more than 90% were obtained. In addition, the area was classified into eight biomass classes. The limited number of areas with *in-situ* measurements on biomass prevented a quantitative evaluation of the accuracy of this classification.

Another classification analysis was performed in Santos et al. (2003). In this study, data from the Brazilian Amazon acquired using the airborne SAR system AeroSensing Radar Systeme (AeS-1) were used to classify part of the imaged area into six land-type classes. Each land-type class was associated with a forest biomass level. An overall classification accuracy of 89% was obtained using P-band SAR data.

AIRSAR data from the Yellowstone National Park, USA, are analysed in Saatchi et al. (2007). This area consists primarily of coniferous forest and sagebrush shrublands, and has strong topographic variability. L- and P-band backscatter data are used to develop regression models for prediction of crown and stem biomass. The regression models include topographic corrections based on the incidence angle (neglecting local ground slope) and the local incidence angle (including local ground slope). The model for stem biomass and the model for crown biomass include seven regression coefficients each. Using a holdout and bootstrap procedure the rmse for estimation of stem biomass was found to be about 20 t/ha ($R^2=0.57$) and 11 t/ha ($R^2=0.81$) for L- and P-band, respectively. The regression models for stem biomass include second order polynomials for all linear polarizations (HH, HV and VV). For estimation of crown biomass the best results were found by combining L- and P-band HV backscatter (first order polynomials including corrections for topography). This model gave an rmse of about 1.9 t/ha ($R^2=0.73$). The study also developed regression models for estimation of canopy fuel variables such as canopy bulk density. Such variables are useful for fire management purposes.

In Saatchi et al. (2011) AIRSAR data from the La Selva Biological Station in Costa Rica are used to develop regression models for biomass estimation. Using inventory data from old growth, secondary succession, and plantation forest, the impact of spatial scale for plot level biomass inventories were investigated. It was found that plot sizes of at least 0.25 ha were required to reduce the coefficient of variation below 20% and give stationary and normal distributions of biomass. For smaller plots single occurrences of sparsely distributed large trees can cause overly large variations in biomass between plots. Regression for biomass estimation models based on polarimetric L- and P-band backscatter, respectively, were developed for the plot sizes 0.25 ha, 0.5 ha and 1.0 ha. Best results were found for the largest spatial scale. The authors conclude that the decreased sensitivity of radar measurements to forest biomass for smaller scales is caused both by increased spatial variability and increased levels of speckle. For 1.0 ha plots the rmse was estimated to be about 20 t/ha for P-band and about 33-40 t/ha for L-band (maximum biomass 270 t/ha, mean biomass 170 t/ha). In this study forest height estimated from C-band interferometry were also added to the regression models, which reduced the rmse by about 40% at L-band and 20% at P-band.

In Neumann et al. (2012) data acquired using E-SAR from the Krycklan catchment in northern Sweden were analysed. This boreal test site has strong topographic variability and biomass at stand level range up to 183 t/ha. L- and P-band backscatter as well as indicators derived from polarimetry and polarimetric interferometry was used to develop methods for biomass estimation. Three methods for biomass estimation were evaluated: multiple linear regression, support vector machine and random forest. The latter two methods are non-parametric. The results suggest that inclusion of indicators beyond backscatter decreased estimation errors by up to about 25% at L-band and 40% at P-band. For these data L-band tends to give lower estimation errors than P-band, which can likely be attributed to topographic effects. Using linear regression the lowest rmse was estimated by cross-validation to be about 20 t/ha. The non-parametric methods did not improve the estimation errors.

4.3.4 SUMMARY OF PAPER III

In paper III data from the BioSAR 2007 campaign are analysed and used to develop models for biomass estimation. In this campaign L- and P-band SAR data were collected from the test site Remningstorp in southern Sweden using the airborne sensor E-SAR. The forest in this site is classified as hemiboreal. Data were collected on three occasions between 9 March 2007 and 2 May 2007. The backscatter from different dates was generally found to be well correlated, although for L-band cases of low correlation were present. For P-band the mean backscatter level increased by about 1 dB from 9 March 2007 to 2 May 2007, which is possibly an effect of increased soil moisture as late winter progress towards spring. Regression models for biomass prediction were developed using reference data consisting of 58 forest stands for which biomass estimates based on laser scanning data were available. Stepwise regression and

an optimisation technique for finding the best response variable transformation were used to derive regression models. The results indicate that the square root of the biomass is proportional to the backscatter expressed in dB. For P-band stepwise regression analysis indicated that inclusion of both HV and HH in the regression model provided a significant improvement compared to models with only one polarization. For L-band inclusion of multiple polarizations did not result in significant improvement. The rmse was evaluated using leave-one-out cross-validation for the 58 forest stands used for model development (training stands, biomass range 10-290 t/ha) as well as ten 80 m by 80 m stands (validation stands, biomass range 50-270 t/ha) for which detailed *in-situ* measurements were available. The latter stands were only used for validation. For L-band the rmse was 40-48 t/ha (31-37%) and 68–83 t/ha (38–46%) for the training and validation stands, respectively. The increased estimation error for the validation stands was largely explained by the higher biomass levels for these stands, since the L-band data showed weaker estimation performance at high biomass levels. For P-band the rmse was estimated to be about 30-35 t/ha (23-27%) and 30-45 t/ha (17-25%) for the training and validation stands, respectively. Models based on HV, HH, and HV and HH gave similar results. For P-band no strong indications of reduced estimation performance for high biomass levels were seen.

4.3.5 SUMMARY OF PAPER IV

In paper IV data from the BioSAR 2007 and the BioSAR 2008 campaigns were used to develop models for biomass retrieval. In BioSAR 2008 E-SAR data were collected from the test site Krycklan in northern Sweden. This boreal test site has pronounced topographic undulations. A new model based on HV backscatter and the HH/VV backscatter ratio is proposed and compared to five other models. The proposed model also includes a correction for ground slope. The models are subjected to three different tests to evaluate estimation performance under different conditions. First, models trained using data from Remningstorp acquired on one of the imaging occasions in 2007 are evaluated using data from the other imaging occasions. Secondly, topographic effects are evaluated by using data from Krycklan. In this test, data from different flight headings were used for training and evaluation. Lastly, models trained using data from one test site were evaluated on the other site. The proposed model performed similar or better than the other models in all of these tests. In particular, the proposed model showed good estimation performance when training was done using data from Krycklan (pronounced topographic variability) and evaluation was done using data from Remningstorp (flat topography). In this case the rmse was estimated to 40-59 t/ha (22-33%), which was lower than for the other models and similar to the error obtained when training was done using data from Remningstorp. When the roles of training and evaluation data were reversed the results are inconclusive since the topographic variations in Remningstorp were insufficient to correctly estimate the slope correction in the proposed model.

4.3.6 DISCUSSION AND CONCLUSIONS

All of the studies summarized in sections 4.3.3 to 4.3.5 agree that UHF-band SAR backscatter is sensitive to forest biomass. There is also a general consensus that P-band is more suitable for biomass estimation than L-band, except in terrain with pronounced topographic variability (Neuman et al., 2012). It can also be concluded that HV and HH polarized backscatter is more sensitive to biomass than VV backscatter. However, there is no consensus on the functional form of the estimation model, and the reported estimation errors vary between different studies. Part of the latter variability can be explained by the different approaches used to estimate biomass and errors. Many studies report residual errors, which tend to be lower than the expected estimation error obtained when predicting biomass on a new dataset (see section 4.3.2). More careful approaches to estimation of errors should be used, as is done in e.g. paper II and especially paper IV. The estimation error also depends on the quality of reference biomass data (e.g. *in-situ* data and laser scanning data) and SAR data. Thus, an important aspect of biomass regression modelling is to analyse and report quality measures for both SAR and reference biomass data (see e.g. paper III). Finally, the estimation error is also dependent on test site conditions (e.g. topography, stand size, and species variability), with lowest estimation errors obtained for flat plantation forests with large mono-species forest stands. However, differences in modelling and evaluation approaches between sites, as well as differences in the quality of both *in-situ* and SAR data, makes it difficult to assess the estimation error as a function of test site conditions based on the published literature. For this purpose new studies covering a range of forest conditions and adopting a consistent approach to regression modelling as well as to collection and processing of reference biomass data and SAR data, are needed.

4.4 BIOMASS CHANGE

Changes in forest biomass through deforestation and degradation leads to a decrease in the carbon pool stored in forests, resulting in outlet of carbon to the atmosphere. On the other hand, growing forest stocks can absorb carbon, thus mitigating the rise of the level of carbon dioxide in the atmosphere. The importance of monitoring biomass change is illustrated by the United Nations initiative for Reducing Emissions through Deforestation and forest Degradation (REDD+). The objective of this initiative is to reduce emissions of carbon dioxide through promotion of sustainable forest management (ESA, 2012). Many studies in which the relation between forest biomass and UHF-band backscatter are analysed have been published. However, studies on biomass change based on UHF data are scarce, and for P-band no such study is available. In paper V, recently acquired P-band SAR data are used to develop models for estimating biomass change.

4.4.1 SUMMARY OF PAPER V

In paper V data from the BioSAR 2007 and BioSAR 2010 campaigns are used to develop regression models for estimation of biomass change. During these campaigns

P-band SAR data from Remningstorp in southern Sweden were collected both during the spring 2007 (9 March to 2 May) and on 23 September 2010. Data from 2007 and 2010 were collected using the airborne systems E-SAR and SETHI, respectively. A method based on the HH/VV backscatter ratio was developed which was able to correct for backscatter changes caused by changes in environmental conditions and calibration errors. After application of this correction method the change in backscatter in areas for which the biomass was the same in 2007 and in 2010 was close to zero. Regression models based on backscatter change were developed using change maps derived from laser scanning data. A two-fold cross-validation approach was used both for model selection and for evaluating differences in estimates based on laser scanning and SAR data. Estimation errors were also evaluated using six 80 m by 80 m plots for which detailed *in-situ* measurements were available both from 2006-2007 and 2010-2011. Different regression models were developed for biomass change on logarithmic, square root and linear scales. The results indicate that the rmse for estimating biomass change is about 15% or 20 t/ha. Simulations were performed in order to evaluate the possibilities of measuring biomass change using spaceborne P-band SAR. The simulations show that it is possible to correctly indicate the sign of the biomass change with 95% probability for the following scenarios: a) 50% change in biomass and 64 ENL, and b) biomass loss of 75% and 8 ENL.

4.4.2 CONCLUSIONS AND OUTLOOK

Monitoring of biomass change on a global scale is an important task for which current methods are inadequate (ESA, 2012). The results in paper V suggest that a spaceborne P-band SAR such as BIOMASS can be useful for estimation of biomass change. The encouraging results from this study should be followed by similar studies to evaluate if the results from paper V hold for other datasets. In particular, studies of biomass change in tropical forest would be very interesting and useful.

4.5 SUMMARY AND CONCLUSIONS

Section 4 have focused primarily on evaluating the usefulness of UHF-band SAR data for estimating forest biomass and forest biomass change. In particular the focus has been on the use of P-band SAR data, since a) the future launch of BIOMASS provides strong motivation for continued efforts on the use of P-band SAR for biomass estimation, and b) many studies have shown that P-band SAR has a stronger potential for biomass mapping than higher frequencies. Paper III lends further evidence to this claim, and suggests that biomass estimation errors in the order of 20-25% at stand level (0.5 ha to 9 ha) can be obtained for (hemi-) boreal forests in flat terrain using airborne P-band SAR data. The results in paper II shows that topography can have a significant impact on P-band SAR images. Thus, it is of great importance to develop methods for correction of topographic effects. A step in this direction was made in paper IV, providing a first order correction for ground slope. The across-site evaluation of predictive performance used in this paper is a very strong method, and paves the way for similar studies. Another important subject which should be further studied is

effects of moisture variability. The results on biomass change estimation presented in paper V are encouraging; however, further studies are needed to confirm that the findings in paper V are repeatable in other areas.

5 CONCLUSIONS AND OUTLOOK

The work in this thesis fits well in the context of biomass mapping using UHF-band SAR data. The conclusion in paper I that Faraday rotation can be measured in fully polarimetric UHF-band SAR data has strong support in other studies, e.g. Freeman (2004), Meyer and Nicoll (2008), and Quegan et al. (2012). The importance of topography for HH-imaging in the UHF-band is recognised (Lin and Sarabandi, 1995). The results in paper II further supports that topography is important, and also shows that small scale topography can have significant effects. The conclusions from paper III adds to the established conclusions that UHF-band backscatter can be used for estimation of forest biomass, that P-band gives lower estimation errors than L-band, and that HV and HH backscatter shows the strongest relations to biomass. Paper IV proposes a new model for biomass estimation based on P-band SAR backscatter data. This model is based partly on findings in previous studies and partly on novel ideas. The across-site evaluation used in this paper is a more difficult test than the single-site evaluations used in most other studies. Novelties are also presented in paper V. This paper is the first to use P-band SAR data for estimation of biomass change. It also proposes a novel method for correction of backscatter changes caused by environmental effects and radiometric calibration uncertainty. The results in this paper are promising, but further studies are needed to validate the results in other areas. In conclusion, the work in this thesis contributes to the growing evidence that UHF-band, and in particular P-band, SAR data can be a useful tool for global biomass mapping. However, it is important to stress that there are limits to the precision and accuracy that can be obtained using such data. An important part of the work in this thesis has been to derive well founded estimates of expected prediction errors.

I would like to conclude this thesis by pinpointing crucial areas in which further research are needed. These areas are identified based on the work in this thesis and on my experience from several years of working with UHF-band SAR in relation to forest biomass. First, the effects of topography on UHF-band SAR data are not yet fully understood. Paper IV provides a first step towards correction of topographic effects, but this correction is not able to capture the full topographic behaviour. The importance of topographic corrections is underlined by recent findings based on tomographic imaging, which suggests that topography can have a strong impact on the cross-polarized channel (Telbaldini and Rocca, 2012). I believe that a deeper understanding of the processes underlying the topographic effects is required to be able to develop improved methods for topographic correction. To this end combined efforts of physical modelling and data analysis methods such as tomography are required. Secondly, the influence of environmental conditions such moisture is a topic which requires further attention. Results in paper IV indicate that corrections for environmental effects are possible using polarimetric data, but further studies are needed to support these findings. Thirdly, the encouraging result that P-band SAR data are well suited for estimation of biomass change needs to be confirmed in additional studies. Fourth and finally, the on-going efforts towards assessing the

performance of a spaceborne P-band SAR should continue. Both system effects (e.g. reduced resolution and increased ambiguity levels compared to airborne system) and effects of the ionosphere must be included. As noted in Quegan et al. (2012) the key issue is not addressing system performance, but rather evaluating the estimation errors for biomass and biomass change. With combined efforts from the SAR community these challenges can be met, and the state of the art can be pushed forward towards new and deeper insight on the possibilities and limitations of monitoring biomass using UHF-band radar systems.

6 REFERENCES

- Akaike, H., (1969), "Fitting autoregressive models for prediction", *Annals of the Institute of Statistical Mathematics* **21**, 243-247.
- Angelliaume, S., Dubois-Fernandez, P., Dreuillet, P., Oriot, H. and Coulombeix, C. (2009), "SETHI, the ONERA airborne SAR sensor, and his low frequency capability", in "Proceedings of the IEEE International Geoscience and Remote Sensing Symposium, 2009", IV-177-IV-179.
- Arlot, S., and Celisse, A. (2010). "A survey of cross-validation procedures for model selection", *Statistics Surveys* **4**, 40-79.
- Askne, J., Dammert, P., Ulander, L. M. H., and Smith, G. (1997), "C-band repeat-pass interferometric SAR observations of the forest", *IEEE Transactions on Geoscience and Remote Sensing* **35**(1), 25-35.
- Askne, J., Santoro, M., Smith, G., and Fransson, J. E. S. (2003), "Multitemporal repeat-pass SAR interferometry of boreal forests", *IEEE Transactions on Geoscience and Remote Sensing* **41**(7), 1540-1550.
- Attema, E. P. W and Ulaby, F. T. (1978), "Vegetation modelled as a water cloud", *Radio Science* **13**, 357-364.
- Baker, J. R., Mitchell, P. L., Cordey, R. A., Groom, G., Settle, J. J. and Stileman, M. R. (1994), "Relationships between physical characteristics and polarimetric radar backscatter for Corsian pine stands in Thetford forest, UK", *International Journal of Remote Sensing* **15**(14), 2827-2849.
- Barton, D. K. (1988), *Modern Radar System Analysis*. Norwood, MA: Artech House.
- Beaudoin, A., Toan, T. L., Goze, S., Nezry, E., Lopes, A., Mougin, E., Hsu, C. C., Han, H. C., Kong, J. A. and Shin, R. T. (1994), "Retrieval of forest biomass from SAR data", *International Journal of Remote Sensing* **15**, 2777-2796.
- Belcher, D. P. (2008), "Theoretical limits on SAR imposed by the ionosphere", *IET Radar, Sonar Navigation* **2**(6), 435-448.
- Bickle, S. H. and Bates, R. T. (1965), "Effects of magneto-ionic propagation on the scattering matrix", *Proceedings of the IEEE* **53**(8), 1089-1091.
- Breiman, L. and Spector, P. (1992), "Submodel selection and evaluation in regression. the x-random case", *International Statistical Review / Revue Internationale de Statistique* **60**(3), pp. 291-319.
- Brown, W. M. (1967), "Synthetic Aperture Radar", *IEEE Transactions on Aerospace and Electronic Systems* **AES-3**(2), 217-229.
- Caicoya, A., Kugler, F., Hajnsek, I. and Papathanassiou, K. (2012), "Boreal forest biomass classification with TanDEM-X", in "Proceedings of the IEEE International Geoscience and Remote Sensing Symposium, 2012", 3439-3442.
- Carrano, C. S., Groves, K. M. and Caton, R. G. (2012), "Simulating the impacts of ionospheric scintillation on L band SAR image formation", *Radio Science* **47**(4).
- Carrara, Walter G., Ron S. Goodman, and Ronald M. Majewski., (1995) *Spotlight Synthetic Aperture Radar - signal processing algorithms*. Boston: Artech House.

- Chen, J. and Quegan, S. (2010), "Improved estimators of faraday rotation in spaceborne polarimetric SAR data", *IEEE Geoscience and Remote Sensing Letters* **7**(4), 846-850.
- Dobson, M., Ulaby, F., Brunfeldt, D., and Held, D. (1986), "External calibration of SIR-B imagery with area-extended and point targets", *IEEE Transactions on Geoscience and Remote Sensing* **GE-24**(4), 453-461.
- Dobson, M., Ulaby, F., LeToan, T., Beaudoin, A., Kasischke, E. and Christensen, N. (1992), "Dependence of radar backscatter on coniferous forest biomass", *IEEE Transactions on Geoscience and Remote Sensing* **30**(2), 412-415.
- Dong, Y. and Richards, J. (1995), "Studies of the cylinder-ground double bounce scattering mechanism in forest backscatter models", *IEEE Transactions on Geoscience and Remote Sensing* **33**(1), 229-231.
- ESA., (2012), "Report for Mission Selection: Biomass", ESA SP-1324/1 (3 volume series). Noordwijk, Netherlands: European Space Agency.
- Eriksson, L. E. B., Santoro, M., Wiesmann, A., and Schmullius, C. (2003), "Multi-temporal JERS repeat-pass coherence for growing stock volume estimation of Siberian forest", *IEEE Transactions on Geoscience and Remote Sensing* **41**(7), 1561-1570.
- Eriksson, L. E. B., (2004), "Satellite-borne L-band interferometric coherence for forestry applications in the boreal zone", PhD thesis, Institute of Geography, Friedrich-Schiller-University, Jena, Germany.
- Folkesson, K. (2008), "Model-based stem volume retrieval and windthrow detection using CARABAS and P-band SAR", PhD thesis, Chalmers University of Technology, Gothenburg, Sweden.
- Folkesson, K., Smith-Jonforsen, G., and Ulander, L. M. (2008), "Validating backscatter models for CARABAS SAR images of coniferous forests", *Canadian Journal of Remote Sensing* **34**(5), 480-495.
- Folkesson, K., Smith-Jonforsen, G. and Ulander, L. M. H. (2009), "Model-based compensation of topographic effects for improved stem-volume retrieval from CARABAS-II VHF-band SAR images", *IEEE Transactions on Geoscience and Remote Sensing* **47**(4), 1045-1055.
- Fransson, J. (1999), "Analysis of synthetic aperture radar images for forestry applications", PhD thesis, Swedish University of Agricultural Sciences, Umeå, Sweden.
- Fransson, J. E. S. and Israelsson, H. (1999), "Estimation of stem volume in boreal forest using ERS-1 C- and JERS-1 L-band SAR data", *International Journal of Remote Sensing* **20**, 123-137.
- Fransson, J. E. S., Walter, F., and Ulander, L. M. H. (2000), "Estimation of forest parameters using CARABAS-II VHF SAR data", *IEEE Transactions on Geoscience and Remote Sensing* **38**(2), 720-727.
- Fransson, J. E. S., Smith, G., Walter, F., Gustavsson, A., and Ulander, L. M. (2004), "Estimation of forest stem volume in sloping terrain using CARABAS-II VHF SAR data", *Canadian Journal of Remote Sensing* **30**(4), 651-660.
- Freeman, A. (1992), "SAR calibration: an overview", *IEEE Transactions on Geoscience and Remote Sensing* **30**(6), 1107-1121.

- Freeman, A. (2004), "Calibration of linearly polarized polarimetric SAR data subject to Faraday rotation", *IEEE Transactions on Geoscience and Remote Sensing* **42**(8), 1617-1624.
- Goldstein, D. (2003), *Polarized Light*, second edition, New York: Marcel Dekker.
- Gray, A., Vachon, P., Livingstone, C., and Lukowski, T. (1990), "Synthetic Aperture Radar calibration using reference reflectors", *IEEE Transactions on Geoscience and Remote Sensing* **28**(3), 374-383.
- Hajnsek, I., Scheiber, R., Ulander, L. M. H., Gustavsson, A., Sandberg, G., Tebaldini, S., Guarnieri, A. M., Rocca, F., Bombardini, F., and Pardini, M. (2008), "BioSAR 2007 technical assistance for the development of airborne SAR and geophysical measurements during the BioSAR 2007 experiment: final report without synthesis", Technical report, European Space Agency, Contract no.: 20755/07/NL/CB.
- Hajnsek, I., Scheiber, R., Keller, M., Horn, R., Lee, S., Ulander, L. M. H., Gustavsson, A., Sandberg, G., Toan, T. L., Tebaldini, S., Guarnieri, A. M., and Rocca, F. (2009), "BioSAR 2008 technical assistance for the development of airborne SAR and geophysical measurements during the BioSAR 2008 Experiment: draft final report – BioSAR campaign", Technical report, European Space Agency, Contract no.: 22052/08/NL/CT.
- Hallberg, B., Smith-Jonforsen, G., and Ulander, L. M. H. (2005), "Measurements on individual trees using multiple VHF SAR images", *IEEE Transactions on Geoscience and Remote Sensing* **43**(10), 2261-2269.
- Hallberg, B. (2007), "Synthetic aperture radar imaging of forests in the VHF and UHF bands: electromagnetic models and data analysis", PhD thesis, Chalmers University of Technology, Gothenburg, Sweden.
- Hellsten, H., Ulander, L. M., Gustavsson, A., and Larsson, B. (1996), Development of VHF CARABAS II SAR, in "Proceedings SPIE 2747, Radar Sensor Technology", 48-60.
- Hersbach, H., Stoffelen, A., and De Haan, S. (2007), "An improved C-band scatterometer ocean geophysical model function: CMOD5", *Journal of Geophysical Research: Oceans* **112**, C03006.
- Hoekman, D. and Quiriones, M. (2000), "Land cover type and biomass classification using AirSAR data for evaluation of monitoring scenarios in the Colombian Amazon", *IEEE Transactions on Geoscience and Remote Sensing* **38**(2), 685-696.
- Hoeting, J. A., Madigan, D., Raftery, A. E., and Volinsky, C. T. (1999), "Bayesian model averaging: a tutorial", *Statistical Science* **14**(4), pp. 382-401.
- Horn, R. (1996), The DLR airborne SAR project E-SAR, in "Proceedings of the International Geoscience and Remote Sensing Symposium, 1996" **3**, 1624-1628.
- Hsu, C. C., Han, H. C., Shin, T., Kong, A., Beaudoin, A., and Toan, T. L. (1994), "Radiative transfer theory for polarimetric remote sensing of pine forest at P-band", *International Journal of Remote Sensing* **15**(14), 2809-2826.
- Imhoff, M. (1995a), "A theoretical analysis of the effect of forest structure on synthetic aperture radar backscatter and the remote sensing of biomass", *IEEE Transactions on Geoscience and Remote Sensing* **33**(2), 341-352.

- Imhoff, M. (1995b), "Radar backscatter and biomass saturation: ramifications for global biomass inventory", *IEEE Transactions on Geoscience and Remote Sensing* **33**(2), 511-518.
- IEEE (2003), "IEEE standard letter designations for radar-frequency bands", *IEEE Std 521-2002 (Revision of IEEE Std 521-1984)*.
- IPCC (2007), *IPCC fourth assesment report: climate change 2007, the physical science basis*, Cambridge, UK: Cambridge University Press.
- Ishimaru, A., Kuga, Y., Liu, J., Kim, Y., and Freeman, T. (1999), "Ionospheric effects on synthetic aperture radar at 100 MHz to 2 GHz", *Radio Science* **34**(1), 257-268.
- Israelsson, H., Askne, J. and Sylvander, R. (1994), "Potential of SAR for forest bole volume estimation", *International Journal of Remote Sensing* **15**(14), 2809-2826.
- Israelsson, H., Ulander, L. M. H., Askne, J., Fransson, J. E. S., Frörlind, P.-O., Gustavsson, A., and Hellsten, H. (1997), "Retrieval of forest stem volume using VHF SAR", *IEEE Transactions on Geoscience and Remote Sensing* **35**(1), 36-40.
- Israelsson, H. (1998), "SAR remote sensing of forests, from microwaves to VHF", PhD thesis, Chalmers University of Technology, Gothenburg, Sweden.
- ITU (2012), "ITU radio regulations, edition of 2012", **1**(2).
- van de Kamp, M., Cannon, P. S., and Terkildsen, M. (2009), "Effect of the ionosphere on defocusing of space-based radars", *Radio Science* **44**, RS1003.
- Karam, M., Fung, A., Lang, R., and Chauhan, N. (1992), "A microwave scattering model for layered vegetation", *IEEE Transactions on Geoscience and Remote Sensing* **30**(4), 767-784.
- Karam, M. A., Amar, F., Fung, A. K., Mougin, E., Lopes, A., Vine, D. M. L., and Beaudoin, A. (1995), "A microwave polarimetric scattering model for forest canopies based on vector radiative transfer theory", *Remote Sensing of Environment* **53**(1), 16-30.
- Koch, B. (2010), "Status and future of laser scanning, synthetic aperture radar and hyperspectral remote sensing data for forest biomass assessment", *Journal of Photogrammetry and Remote Sensing* **65**(6), 581-590.
- Kononov, A. and Ka, M.-H. (2008), "Model-associated forest parameter retrieval using VHF SAR data at the individual tree level", *IEEE Transactions on Geoscience and Remote Sensing* **46**(1), 69-84.
- Kononov, A., Wyholt, A., Sandberg, G., and Ulander, L. M. H. (2011), "Statistical analysis of VHF-band tree backscattering using forest ground truth data and PO scattering model", *IEEE Transactions on Geoscience and Remote Sensing* **49**(8), 3035-3046.
- Kvålseth, T. O. (1985), "Cautionary note about R^2 ", *The American Statistician* **39**(4), 279-285.
- Le Toan, T., Beaudoin, A., Riou, J. and Guyon, D. (1992), "Relating forest biomass to SAR data", *IEEE Transactions on Geoscience and Remote Sensing* **30**(2), 403-411.
- Lefsky, M. A., Harding, D. J., Keller, M., Cohen, W. B., Carabajal, C. C., Del Bom Espirito-Santo, F., Hunter, M. O., and de Oliveira, Raimundo, J. (2005), "Estimates of

- forest canopy height and aboveground biomass using ICESat”, *Geophysical Research Letters* **32**, L22S02.
- Liang, P., Moghaddam, M., Pierce, L., Lucas, R. (2005), “Radar backscattering model for multilayer mixed-species forests”, *IEEE Transactions on Geoscience and Remote Sensing* **43**(11), 2612-2626.
- Lin, Y.-C. and Sarabandi, K. (1995), “Electromagnetic scattering model for a tree trunk above a tilted ground plane”, *IEEE Transactions on Geoscience and Remote Sensing* **33**(4), 1063-1070.
- Lin, Y.-C. and Sarabandi, K. (1999), “A Monte Carlo coherent scattering model for forest canopies using fractal-generated trees”, *IEEE Transactions on Geoscience and Remote Sensing*, **37**(1), 440-451.
- Liu, J., Kuga, Y., Ishimaru, A., Pi, X., and Freeman, A. (2003), “Ionospheric effects on SAR imaging: a numerical study”, *IEEE Transactions on Geoscience and Remote Sensing* **41**(5), 939-947.
- Long, A. E. (1995), “C-band V-polarized radar sea-echo model from ERS-1 Haltenbanken campaign”, *Journal of Electromagnetic Waves and Applications* **9**(3), 371-391.
- Lopez-Sanchez, J., Esteban-Gonzalez, H., Baquero-Escudero, M., and Fortuny-Guasch, J. (1999), “An electromagnetic scattering model for multiple tree trunks above a tilted rough ground plane”, *IEEE Transactions on Geoscience and Remote Sensing* **37**(2), 659-667.
- Mallows, C. L. (1973), “Some comments on CP”, *Technometrics* **15**(4), 661-675.
- Melon, P., Martinez, J.-M., Le Toan, T., Ulander, L. M. H., and Beaudoin, A. (2001), “On the retrieving of forest stem volume from VHF SAR data: observation and modeling”, *IEEE Transactions on Geoscience and Remote Sensing* **39**(11), 2364-2372.
- Meyer, F. J. and Nicoll, J. B. (2008), “Prediction, detection, and correction of faraday rotation in full-polarimetric L-Band SAR data”, *IEEE Transactions on Geoscience and Remote Sensing* **46**(10), 3076-3086.
- Neumann, M., Saatchi, S. S., Ulander, L. M. H. and Fransson, J. E. S. (2012), “Assessing performance of L- and P-band polarimetric interferometric SAR data in estimating boreal forest above-ground biomass”, *IEEE Transactions on Geoscience and Remote Sensing* **50**(3), 714 -726.
- Oliver, C., and Quegan, S. (2004), *Understanding Synthetic Aperture Radar Images*, Raleigh, NC: SciTech Publishing.
- Picard, G., Le Toan, T., Quegan, S., Caraglio, Y., and Castel, T. (2004), “Radiative transfer modeling of cross-polarized backscatter from a pine forest using the discrete ordinate and eigenvalue method”, *IEEE Transactions on Geoscience and Remote Sensing* **42**(8), 1720-1730.
- Picard, R. R. and Cook, R. D. (1984), “Cross-validation of regression models”, *Journal of the American Statistical Association* **79**(387), 575-583.
- Qi, R.-Y. and Jin, Y.-Q. (2007), “Analysis of the effects of Faraday rotation on spaceborne polarimetric SAR observations at P-band”, *IEEE Transactions on Geoscience and Remote Sensing* **45**(5), 1115-1122.

- Quegan, S., Rogers, N., Papathanassiou, K., Kim, J. S., Rocca, F., Tebeldini, S. (2012), "Study of ionospheric disturbance mitigation schemes, Final Report", Technical report, European Space Agency, Contract no.: 22849/09/NL/JA/ef.
- Quilfen, Y., Chapron, B., Elfouhaily, T., Katsaros, K., and Tournadre, J. (1998), "Observation of tropical cyclones by high-resolution scatterometry", *Journal of Geophysical Research: Oceans* **103**(C4) 7767-7786.
- Ranson, K. and Sun, G. (1994), "Mapping biomass of a northern forest using multifrequency SAR data", *IEEE Transactions on Geoscience and Remote Sensing* **32**(2), 388-396.
- Ranson, K., Sun, G., Weishampel, J. and Knox, R. (1997), "Forest biomass from combined ecosystem and radar backscatter modeling", *Remote Sensing of Environment* **59**(1), 118-133.
- Rauste, Y., Häme, T., Pulliainen, J., Heiska, K. and Hallikainen, M. (1994), "Radar-based forest biomass estimation", *International Journal of Remote Sensing* **15**, 1797-2808.
- Rawlings, J. O., Pantula, S. G., and Dickey, D. A. (1998), *Applied regression analysis: a research tool*, second edition, New York: Springer.
- Rignot, E., Way, J., Williams, C. and Viereck, L. (1994), "Radar estimates of aboveground biomass in boreal forests of interior Alaska", *IEEE Transactions on Geoscience and Remote Sensing* **32**(5), 1117-1124.
- Rignot, E., Zimmermann, R. and van Zyl, J. (1995), "Spaceborne applications of P band imaging radars for measuring forest biomass", *IEEE Transactions on Geoscience and Remote Sensing* **33**(5), 1162-1169.
- Rogers, N., and Quegan, S., and Kim, J. and Papathanassiou, K. (2013), "Impacts of ionospheric scintillation on the BIOMASS P-Band satellite SAR", *IEEE Transactions on Geoscience and Remote Sensing*, available online.
- Rogers, N. and Quegan, S. (2013), "Faraday rotation correction for the ESA BIOMASS P-band synthetic aperture radar", in "Proceedings of the 7th European Conference on Antennas and Propagation", 3919-3923.
- Rosenqvist, A., Shimada, M., Ito, N., and Watanabe, M. (2007), "ALOS PALSAR: a pathfinder mission for global-scale monitoring of the environment", *IEEE Transactions on Geoscience and Remote Sensing* **45**(11), 3307-3316.
- Saatchi, S. and McDonald, K. (1997), "Coherent effects in microwave backscattering models for forest canopies", *IEEE Transactions on Geoscience and Remote Sensing* **35**(4), 1032-1044.
- Saatchi, S., Halligan, K., Despain, D. and Crabtree, R. (2007), "Estimation of forest fuel load from radar remote sensing", *IEEE Transactions on Geoscience and Remote Sensing* **45**(6), 1726-1740.
- Saatchi, S., Marlier, M., Chazdon, R. L., Clark, D. B. and Russell, A. E. (2011), "Impact of spatial variability of tropical forest structure on radar estimation of aboveground biomass", *Remote Sensing of Environment* **115**(11), 2836-2849.

- Santoro, M., Askne, J., Smith, G., and Fransson, J. E. S. (2002), "Stem volume retrieval in boreal forests from ERS-1/2 interferometry", *Remote Sensing of Environment* **81**(1), 19 - 35.
- Santoro, M., Fransson, J. E. S., Eriksson, L., Magnusson, M., Ulander, L., and Olsson, H. (2009), "Signatures of ALOS PALSAR L-Band backscatter in Swedish forest", *IEEE Transactions on Geoscience and Remote Sensing* **47**(12), 4001-4019.
- Santoro, M., Beer, C., Cartus, O., Schmullius, C., Shvidenko, A., McCallum, I., Wegmüller, U., and Wiesmann, A. (2011), "Retrieval of growing stock volume in boreal forest using hyper-temporal series of Envisat ScanSAR backscatter measurements", *Remote Sensing of Environment* **115**(2), 490-507.
- Santoro, M., Cartus, O., Fransson, J. E. S., Shvidenko, A., McCallum, I., Hall, R. J., Beaudoin, A., Beer, C., and Schmullius, C. (2013), "Estimates of forest growing stock volume for Sweden, central Siberia, and Québec using Envisat Advanced Synthetic Aperture Radar backscatter data", *Remote Sensing* **5**(9), 4503-4532.
- Santos, J. R., Freitas, C. C., Araujo, L. S., Dutra, L. V., Mura, J. C., Gama, F. F., Soler, L. S. and Sant'Anna, S. J. (2003), "Airborne P-band applied to the aboveground biomass studies in the Brazilian tropical rainforest", *Remote Sensing of Environment* **87**(4), 482-493.
- Schwartz, G., (1978), "Estimating the dimension of a model", *Annals of Statistics* **6**, 461-464.
- Shao, J. (1993), "Linear model selection by cross-validation", *Journal of the American Statistical Association* **88**(422), 486-494.
- Shimada, M., Muraki, Y., and Otsuka, Y. (2008), Discovery of anomalous stripes over the Amazon by the PALSAR onboard ALOS satellite, in "Proceedings of the IEEE International Geoscience and Remote Sensing Symposium, 2008", II-387-II-390.
- Shimada, M., Isoguchi, O., Tadono, T., and Isono, K. (2009), "PALSAR radiometric and geometric calibration", *IEEE Transactions on Geoscience and Remote Sensing* **47**(12), 3915-3932.
- Skolnik, M. I. (1990), *Radar Handbook*, second edition, New York: McGraw Hill.
- Small, D., Holecz, F., Meier, E., and Nuesch, D. (1998), "Absolute radiometric correction in rugged terrain: a plea for integrated radar brightness", in "Proceedings of the International Geoscience and Remote Sensing Symposium, 1998" **1**, 330-332.
- Smith, G. (2000), "Radar remote sensing of forests using CARABAS and ERS", PhD thesis, Chalmers University of Technology, Gothenburg, Sweden.
- Smith, G. and Ulander, L. M. H. (2000), "A model relating VHF-band backscatter to stem volume of coniferous boreal forest", *IEEE Transactions on Geoscience and Remote Sensing* **38**(2), 728-740.
- Smith-Jonforsen, G., Ulander, L., and Luo, X. (2005), "Low VHF-band backscatter from coniferous forests on sloping terrain", *Geoscience and Remote Sensing, IEEE Transactions on* **43**(10), 2246 - 2260.
- Smith-Jonforsen, G., Folkesson, K., Hallberg, B., and Ulander, L. (2007), "Effects of forest biomass and stand consolidation on P-band backscatter", *IEEE Transactions on Geoscience and Remote Sensing Letters* **4**(4), 669-673.

- Stoffelen, A. (1998), "Toward the true near-surface wind speed: error modeling and calibration using triple collocation", *Journal of Geophysical Research: Oceans* **103**(3334), 7755-7766.
- Sullivan, R. J. (2004), *Radar foundations for imaging and advanced concepts*, Raleigh, NC: SciTech Publishing Inc.
- Sun, G., Simonett, D. S., and Strahler, A. (1991), "A radar backscatter model for discontinuous coniferous forests", *IEEE Transactions on Geoscience and Remote Sensing* **29**(4), 639-650.
- Tebaldini, S. and Rocca, F. (2012), "Multibaseline polarimetric SAR tomography of a boreal forest at P- and L-Bands", *IEEE Transactions on Geoscience and Remote Sensing* **50**(1), 232 -246.
- Thirion, L., Colin, E., and Dahon, C. (2006), "Capabilities of a forest coherent scattering model applied to radiometry, interferometry, and polarimetry at P- and L-band", *IEEE Transactions on Geoscience and Remote Sensing* **44**(4), 849-862.
- Torgovnikov, G. I. (1993), *Dielectric properties of wood and wood-based materials*, Berlin: Springer.
- Ulaby, F. T., Moore, R. K., and Fung, A. K. (1982), *Microwave remote sensing – Active and passive, Volume II*, Norwood, MA: Artech House
- Ulaby, F.T., Sarabandi, K., McDonald, K., Whitt, M., and Dobson, M. C., (1990) "Michigan Microwave Canopy Scattering Model", *International Journal of Remote Sensing* **11**(7), 1223-1253.
- Ulander, L. M. H. (1991a), "Accuracy of using point targets for SAR calibration", *IEEE Transactions on Aerospace Electronic Systems* **27**(1), 139-148.
- Ulander, L. M. H. (1991b), "Radar remote sensing of sea ice: measurements and theory", PhD thesis, Chalmers University of Technology, Gothenburg, Sweden.
- Ulander, L. M. H. (1996), "Radiometric slope correction of synthetic-aperture radar images", *IEEE Transactions on Geoscience and Remote Sensing* **34**(5), 1115-1122.
- Ulander, L. M. H. and Hellsten, H. (1996), "A new formula for SAR spatial resolution", *AEU International Journal of Electronics and Communications*. **50**(2), 117-121.
- Ulander, L. M. H., Blom, M., Flood, B., Follo, P., Frolind, P.-O., Gustavsson, A., Jonsson, T., Larsson, B., Murdin, D., Pettersson, M., Raaf, U., and Stenstrom, G. (2003), Development of the ultra-wideband LORA SAR operating in the VHF/UHF-band, in "Proceedings of the IEEE International Geoscience and Remote Sensing Symposium, 2003", 4268-4270 vol.7.
- Ulander, L. M. H., Gustavsson, A., Flood, B., Murdin, D., Dubois-Fernandez, P., Depuis, X., Sandberg, G., Soja, M. J., Eriksson, L. E. B., Fransson, J. E. S., Holmgren, J., and Wallerman, J. (2011), "BioSAR 2010 technical assistance for the development of airborne SAR and geophysical measurements during the BioSAR 2010 experiment: final report", Technical report, European Space Agency, Contract no.: 4000102285/10/NL/JA/ef.

- Vu, V.-T., Sjögren, T., Pettersson, M., and Hellsten, H. (2010), “An impulse response function for evaluation of UWB SAR imaging”, *IEEE Transactions on Signal Processing* **58**(7), 3927-3932.
- Vu, V.-T., Sjögren, T., and Pettersson, M. (2012), “On Synthetic Aperture Radar azimuth and range resolution equations”, *IEEE Transactions on Aerospace and Electronic Systems* **48**(2), 1764-1769.
- Woodhouse, I. (2006), “Predicting backscatter-biomass and height-biomass trends using a macroecology model”, *IEEE Transactions on Geoscience and Remote Sensing* **44**(4), 871-877.
- Wright, P. A., Quegan, S., Wheadon, N. S., and Hall, C. D. (2003), “Faraday rotation effects on L-band spaceborne SAR data”, *IEEE Transactions on Geoscience and Remote Sensing* **41**(12), 2735-2744.
- Xu, Z.-W., Wu, J., and Wu, Z.-S. (2004), “A survey of ionospheric effects on space-based radar”, *Waves in Random Media* **14**(2), S189-S273.
- Xu, Z.-W., Wu, J., and Wu, Z.-S. (2008), “Potential Effects of the Ionosphere on Space-Based SAR Imaging”, *IEEE Transactions on Antennas and Propagation* **56**(7), 1968-1975.
- Zhang, P. (1993), “Model Selection Via Multifold Cross Validation”, *The Annals of Statistics* **21**(1), pp. 299-313.
- van Zyl, J. (1990), “Calibration of polarimetric radar images using only image parameters and trihedral corner reflector responses”, *IEEE Transactions on Geoscience and Remote Sensing* **28**(3), 337-348.